

Two Different Long-term Behaviors in Black-Hole Candidates: Evidence for Two Accretion Flows?

D. M. Smith¹, W. A. Heindl², J. H. Swank³

ABSTRACT

We discuss the results of long-term hard x-ray monitoring of Galactic black-hole candidates 1E 1740.7–2942, GRS 1758–258, Cyg X–1, GX 339–4, and Cyg X–3 with the *Rossi X-Ray Timing Explorer (RXTE)*. The objects divide into two classes. In the first class, exemplified by Cyg X–1, luminosity and spectral hardness evolve simultaneously. In the second class, the relation is more complicated: the softest spectra occur while the count rate is dropping. Most models of accretion, tailored to Cyg X–1, do not predict the second sort of behavior. One interpretation is a simple model with two simultaneous, independent accretion flows: a thin disk and a hot halo. A drop in the accretion rate affecting both flows would propagate through the halo immediately but might take up to several weeks to propagate through the disk. While the inner halo is thus temporarily depleted compared to the disk, a temporary soft state is expected. This picture is supported by the observation that those sources which show delays (1E 1740.7–2942, GRS 1758–258, and GX 339–4) are expected to have low-mass companions, and those which do not (Cyg X–1, Cyg X–3) are known or thought to have high-mass companions. Low-mass companions imply accretion by Roche-lobe overflow, with a high specific angular momentum in the accreting material, and therefore a large disk with a long viscous timescale. Wind accretion from massive companions is expected to result in a much smaller disk, and thus little viscous delay.

Subject headings: accretion, accretion disks — black hole physics — x-rays:stars — stars,individual:(1E 1740.7-2942) — stars,individual:(GRS 1758-258) — stars,individual:(GX 339-4) — stars,individual:(Cyg X-1) — stars,individual:(Cyg X-3)

¹Space Sciences Laboratory, University of California Berkeley, Berkeley, CA 94720

²Center for Astrophysics and Space Sciences, Code 0424, University of California San Diego, La Jolla, CA 92093

³NASA Goddard Space Flight Center, Code 666, Greenbelt, MD 20771

1. Introduction

Among the x-ray binaries which are identified as black-hole candidates by their mass functions, only three show persistent bright emission: Cyg X–1, LMC X–3, and LMC X–1. At least two more non-transient Galactic objects are usually considered black-hole candidates by courtesy due to the similarity of their hard x-ray behavior to that of Cyg X–1: 1E 1740.7–2942 and GRS 1758–258. GX 339–4 occupies a position intermediate between persistent and transient sources, being bright a significant fraction of the time but quiescent more often. The optical counterparts of the latter three systems have not been detected due to their distance, extinction by Galactic dust, and, in the case of GX 339–4, dominance of the accretion-disk’s optical emission.

GRS 1758–258 almost certainly has a low or intermediate mass companion, and is therefore likely to be accreting by Roche-lobe overflow, in contrast to Cyg X–1, which is thought to accrete the wind from its O supergiant companion. K-band observations of GRS 1758–258 (Martí et al. 1998) show that the two brightest stars consistent with the Very Large Array (VLA) radio position appear to be a low-mass K-type red giant and a main-sequence F star; more massive stars, which might fuel wind accretion, are ruled out.

For 1E 1740.7–2942, Mirabel et al. (1991) suggested a companion later than B2, but their argument was indirect. The upper limit was on 6 cm radio flux; UV from an earlier companion would produce so much ionization in a positionally coincident molecular cloud that a compact HII region would have been seen with the VLA. This argument relies on 1E 1740.7–2942 being within the cloud and not behind or in front of it. HCO⁺ emission-line observations have been used to argue that it is indeed within the cloud (Philips & Lazio 1995; Yan & Dalgarno 1997), but the small amplitude of the 6.4 keV iron fluorescence line from the source has been used to argue that it is behind the cloud (Churazov, Gilfanov & Sunyaev 1996) or in front of it (Sakano et al. 1999). The deepest K-band observations near 1E 1740.7–2942 were recently made with the Very Large Telescope (VLT) of the European Southern Observatory (Martí et al. 2000). Four stars of K magnitude 18.5–19.0 are about 1” from the VLA position, and each might represent a massive companion. Martí et al. (2000) found that the K-band 3σ upper limit exactly at the VLA position (19.5) would constrain the companion to be a main sequence star later than about B8 V or a giant earlier than G5 III. The conclusion awaits improvement of the 1” uncertainty in the alignment of the VLA and VLT fields. Since 1E 1740.7–2942 shares the characteristic of bright, extended radio jets with GRS 1758–258 and not Cyg X–1, one might argue (independent of the evidence presented below) that it is more likely to be similar to GRS 1758–258 overall, i.e. to be a Roche-lobe accretor.

Optical emission has been seen frequently from GX 339–4, which shows less absorption

than either 1E 1740.7–2942 or GRS 1758–258, and is probably closer. The optical spectrum has always been consistent with an accretion disk, however, so there has been no spectral classification of the companion. Optical observations taken when the x-ray luminosity was very low (Callanan et al. 1992) imply an upper limit of $(0.6 \pm 0.2) L_{\odot}$ for the companion at the farthest estimated distance of 4 kpc (Cowley et al. 1987; Zdziarski et al. 1998) and one tenth of that at the closest estimated distance of 1.3 kpc (Predehl et al. 1991). Zdziarski et al. (1998) derived a somewhat higher extinction ($A_v = 3.4 - 4$) than that taken by Callanan et al. (1992) from Ilovaisky et al. (1986) ($A_v = 2.2$), which would increase the upper limit to about $3 L_{\odot}$. Even at this highest upper limit, the companion cannot be a high-mass star providing a significant wind.

The unique x-ray binary Cyg X–3 has been interpreted as a black hole in a 4.8 hr orbit with a Wolf-Rayet star (Schmutz et al. 1996; van Kerkwijk et al. 1996), but this identification of both components has been questioned (Mittra 1996, 1998). A Wolf-Rayet star could provide sufficient material in its wind to feed a bright x-ray binary system.

Cyg X–1, 1E 1740.7–2942, GRS 1758–258, and GX 339–4 spend most of their time in the spectral state called “hard” or “low”. This state, one of the two canonical states of black-hole candidates at moderate luminosity, is characterized by a hard power law (photon index 1.4 to 1.9) with an exponential rollover around 100 keV. The other canonical state, “soft” or “high”, is characterized by a softer power law with no exponential cutoff, plus a thermal component with a temperature on the order of 1 keV which can dominate the overall luminosity. There can be a gradual transition between these canonical states, now usually called an intermediate state (Méndez and van der Klis 1997). It has recently been discovered, however, that at least one property of this state is not intermediate at all: Pottschmidt et al. (2000) found that the lags between rapid variations in soft and hard flux are far longer during state transitions of Cyg X–1 than in either the soft or hard states. The “very high” state, characterized by high accretion rates and more complicated behaviors, is beyond the scope of this paper, never having been displayed by Cyg X–1, 1E 1740.7–2942 or GRS 1758–258.

One common picture of accretion in these systems is a standard thin accretion disk at large radii, which is truncated at some inner radius and replaced by a hot, more spherical flow (e.g., Shapiro et al. 1976). The thin disk produces thermal emission and the hot flow scatters it up into a power law. The transition from the low state to the high state is thought to occur when the accretion rate increases, with the result that the transition radius moves inward until the thin disk extends all the way down to the last stable orbit allowed by general relativity (e.g., Esin et al. 1998; Janiuk, Życki & Czerny 2000).

In this paper we will demonstrate that this picture, although adequate to explain the behavior of Cyg X–1, will have to be altered to address the more complicated evolution of

luminosity and spectrum in other black-hole candidates.

2. Results

2.1. Observations

Cyg X–1, Cyg X–3, 1E 1740.7–2942, GRS 1758–258, and GX 339–4 have been monitored by the *Rossi X-Ray Timing Explorer (RXTE)* since the start of science operations in 1996 February. Cyg X–1, Cyg X–3, and GX 339–4 are bright enough to be monitored by the All-Sky Monitor (ASM) instrument, and we have used quick-look results provided by the ASM team. 1E 1740.7–2942 and GRS 1758–258, which are fainter and in a crowded part of the sky, have been monitored by periodic visits with the highly-sensitive Proportional Counter Array (PCA) instrument (Jahoda et al. 1996).

The PCA monitoring observations, which last about 1500 s each, occurred monthly during 1996, weekly until early this year, and are now begin taken twice per week. There are data gaps from November to January every year due to a constraint against pointing the PCA near the Sun. In Main et al. (1999, hereafter Paper I) and Smith et al. (1997) we discussed the details of our observing strategy for 1E 1740.7–2942 and GRS 1758–258, including offset-pointing to avoid nearby sources and subtraction of Galactic diffuse emission. The principal changes since Paper I was written are the new data acquired and a reanalysis of the whole data set using updated PCA response and background models (the new faint source model).

Figure 1 shows the count rate and best-fit power-law index (PLI) in photon space as a function of time for 1E 1740.7–2942 and GRS 1758–258. The count rate is in the range 2.5 - 25 keV, uncorrected for interstellar absorption or instrument response. The PLI was fitted to the data in the same range.

Figure 2 shows ASM data for Cyg X–1. To restrict our attention to the power-law component of the emission rather than the disk blackbody, we sum only ASM channels 2 (3.0-5.0 keV) and 3 (5.0-12.1 keV). To match the 1E 1740.7–2942 and GRS 1758–258 data as closely as possible, we plot weekly accumulations of ASM data. Figure 2a shows the sum of the count rate in these two channels as a measure of the source flux. Figure 2b shows the ratio of these two channels.

We used weekly PCA pointings to Cyg X–1 in 1998 to find the true PLI for comparison with contemporaneous ASM data. Figure 3 shows an expanded view of the ASM data with the PCA data superimposed. The count rates (Figure 3a) are for ASM channels 2+3 and

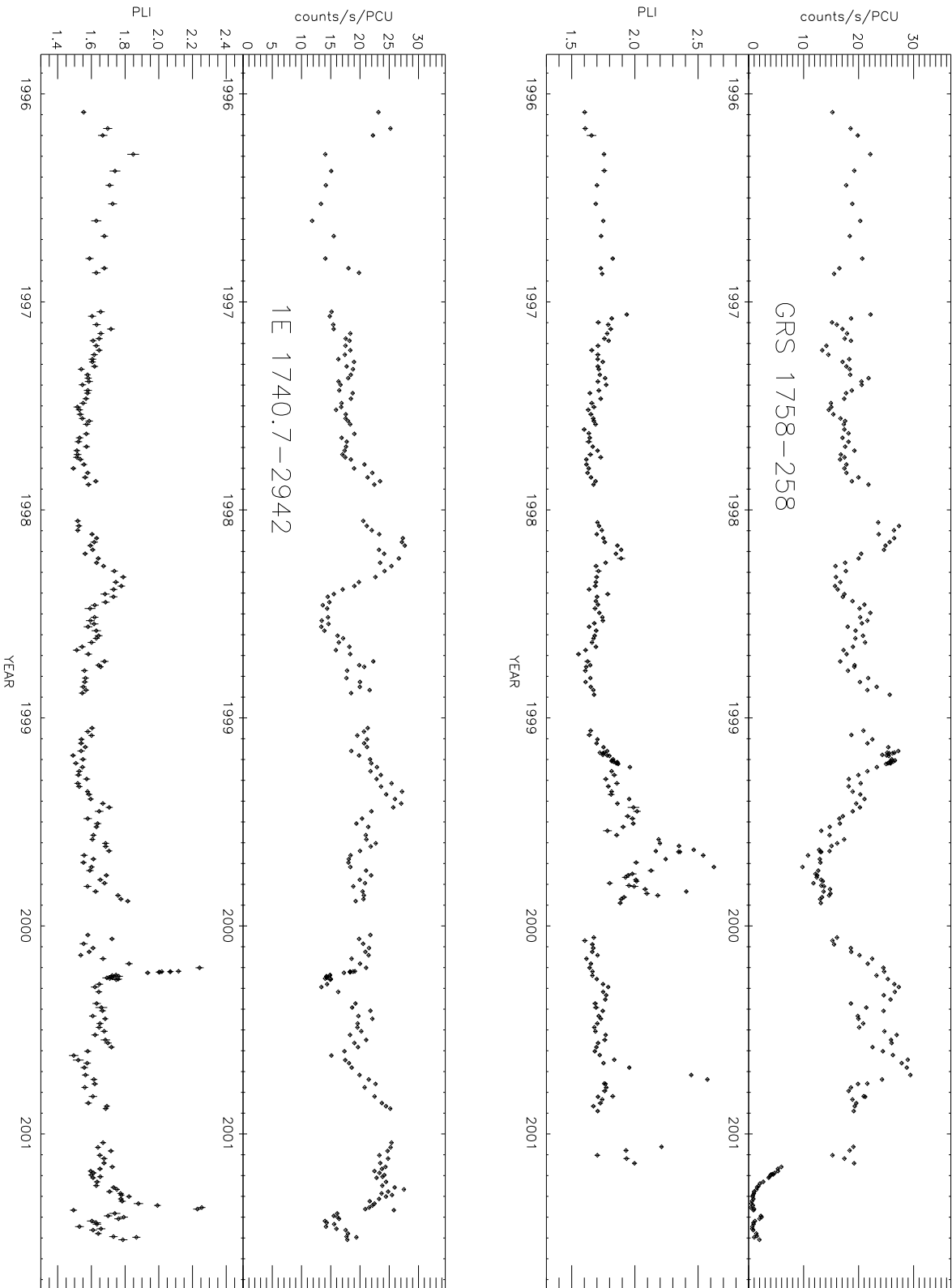


Fig. 1.— Count rate and power law index from GRS 1758-258 and 1E 1740.7-2942 as a function of time from *RXTE* monitoring data.

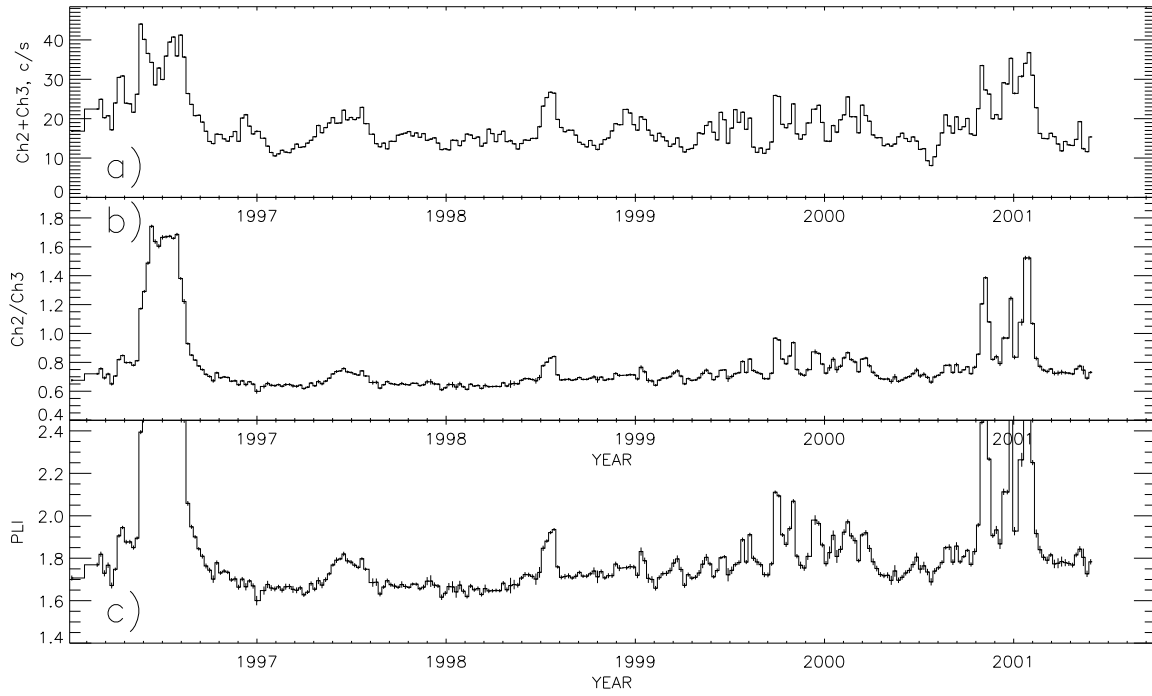


Fig. 2.— Summed count rate in channels 2 and 3, ratio between channels 2 and 3, and derived power law index in Cyg X-1 from *RXTE* ASM data.

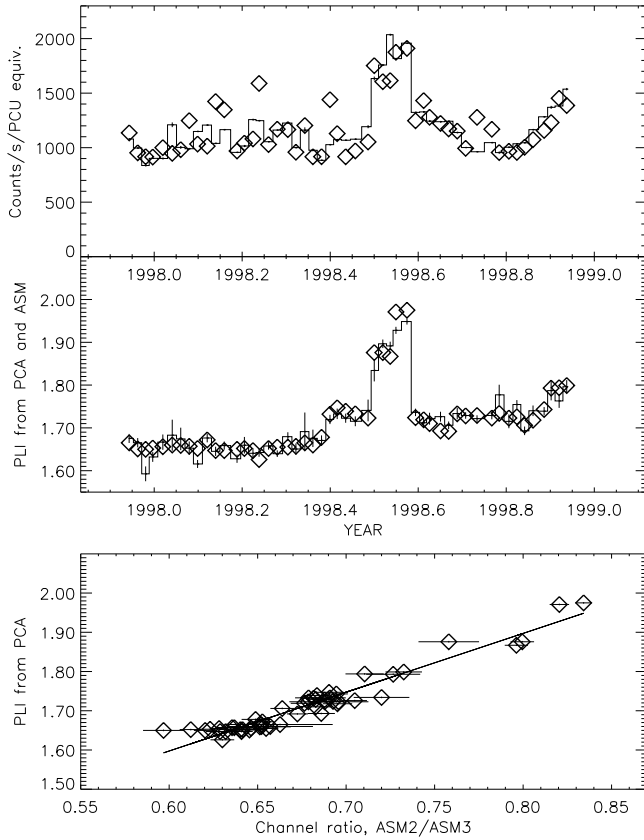


Fig. 3.— *RXTE* ASM data (histograms) and PCA data (points) for Cyg X–1 during 1998. Top: count rates. The PCA data (diamonds) are in counts/second/PCU from 3–12 keV, the ASM energy range. The PCA error bars are much smaller than the plotting symbols. The ASM count rates (histogram) have been normalized to have the same average value as the PCA data. Middle: Fitted PLI from the PCA data (diamonds) and equivalent index derived from the ASM data by equation 1 (histogram). The PCA error bars are comparable to the size of the plotting symbol. Bottom: The same data points as in the middle plot, but with the PCA PLI plotted against the ASM count ratio, showing the linear fit (equation 1).

for the PCA data restricted to the same range (3.0-12.1 keV). The PCA data show more variation not because of statistical errors, which are far smaller than the plotting symbols used, but because they represent a single (3000 s) snapshot instead of the average of a series of snapshots taken over a week, as is the case with the ASM data. This indicates a significant power at frequencies between about 1 and 300 μHz , an interesting phenomenon beyond the scope of this paper.

Figure 3b compares the PCA PLI with the best-fit linear transform of the ASM channel ratio using this data set. This relation between the PLI and the ratio, R , of ASM channels 2 and 3 (Figure 2b) is

$$\text{PLI} = 1.499R + 0.698. \quad (1)$$

Figure 3c shows the PLI from the PCA data plotted against the ASM channel ratio for this data set, and the fit that gives equation 1. We do not expect that this relation applies for the softest data of Figure 2, where the disk blackbody emission could dominate channel 2, since this did not occur in 1998. The derived PLI, shown in Figure 2c, should therefore not be considered accurate when it is softer than about 2.1.

Figure 4 shows the ASM count rate and channel ratio for GX 339–4. Since this source is much fainter than Cyg X–1, and sometimes drops to undetectable levels, the data are poorer. The ASM coverage of any given point in the sky is irregular, so when the data are accumulated on a weekly basis as in Figure 2, there are periods where the statistics are so poor that a plot of the data is difficult to interpret. We therefore produced Figure 4 by accumulating sets of 50 consecutive ASM snapshots and averaging them together. One clear state transition can be seen in 1998. Unfortunately, the transitions into and out of the soft state both occurred around January, when the *RXTE* pointing schedule, driven by a Sun-angle constraint, results annually in very poor coverage of the Galactic Center region by the ASM.

Finally, Figure 5 shows the ASM rate and ratio data for Cyg X–3, with one-week accumulations as in Figure 2. The hard x-ray spectra of this source are more complicated than the others, including variable absorption and a very bright iron line, presumably due to the effects of a very dense wind from its companion (e.g., Nakamura et al. 1993). We have therefore not attempted to convert the channel 2 to channel 3 ratio into a power-law index, but we leave it as the measure of softness for this source.

2.2. Correlating Photon Flux and Spectral Index

There is a strong contrast in the behaviors shown in Figures 1 and 2. In Cyg X–1, the curves of brightening and softening appear almost identical, while they have a very different time-dependence in GRS 1758–258 and 1E 1740.7–2942. This phenomenon is the principal result of this paper. In order to make the relations between these quantities clearer in all three sources, we have derived Figures 6-9 from the raw data in Figures 1 and 2. These figures compare the PLI with both the photon flux and the time derivative of the photon flux for each source. In order to produce a set of standard comparisons, the count rates have had the instrumental responses and interstellar absorption removed and they are extrapolated to the range 2-100 keV using the fitted PLI. This range was chosen to represent the total photon flux in the power law part of the spectrum of each source. Above 100 keV the photon flux is small for both hard and soft state spectra, and below 100 keV the error introduced in the hard state by ignoring the exponential rolloff is also small. The flux derivatives were calculated at a given time by fitting a line to all the data within 15 days of that point and using the slope. For visual comparison, the PLI, flux, and flux derivative curves are all scaled to have a mean of zero and an rms of one.

The last panel of each figure shows the cross-correlation between the curves in each of the two panels above it. The peak correlations (positive or negative) and corresponding lags are shown in Table 1. A positive lag is defined as the PLI lagging behind the other quantity. To cross-correlate the unevenly sampled data, we interpolated between points on the PLI curve in order to get values at times corresponding to the shifted flux and flux derivative data.

The errors in the values of the correlation coefficient and the best-fit lag were estimated empirically. All points in the flux and PLI curves were randomly perturbed according to a Gaussian distribution with a width determined by the errors of the measurements. The analysis process, including calculation of the flux derivative and cross-correlation, was then repeated for the perturbed data set. This was done 1000 times with different random perturbations for each cross-correlation. The errors quoted on the correlation coefficients and the best-fit lags are the intervals that enclosed 95% of the results from the perturbed cases.

To make the results in Table 1 as mutually comparable as possible, we averaged the ASM data for Cyg X–1 and Cyg X–3 into time intervals centered on the times of each of the PCA pointings to 1E 1740.7–2942, so that the number of data points and irregularity of sampling is similar for all four sources. Figures 6, 7 and later figures for Cyg X–1 and Cyg X–3 use regular weekly binning of the data for display (as do Figures 2 and 5). Using these weekly bins or using daily bins, the cross-correlation results are still similar to Table 1. For Cyg X–3 the ratio between ASM channels 2 and 3 is used as a surrogate for the PLI.

Table 1. Cross-correlation peak values and peak lags, for pairs of quantities $Q1$ and $Q2$

Q1	Q2	Cyg X-1		Cyg X-3		1E 1740.7-2942		GRS 1758-258	
		Value	Lag (dy)	Value	Lag (dy)	Value	Lag (dy)	Value	Lag (dy)
γ^a	C^b	0.803 ± 0.016	-1.2 ± 2.0	0.906 ± 0.016	-2.9 ± 3.3	-0.426 ± 0.026	-25.45 ± 0.15	-0.596 ± 0.020	-60.2 ± 6.6
γ	F^c	0.871 ± 0.014	0.3 ± 1.9	-0.459 ± 0.038	-25.4 ± 2.5	-0.587 ± 0.026	-60.0 ± 8.0
γ	E^d	0.874 ± 0.013	0.0 ± 2.4	-0.632 ± 0.037	-11.3 ± 2.1	-0.712 ± 0.021	-24 ± 22
γ	$-dC/dt$	0.327 ± 0.028	-13.4 ± 1.2	-0.471 ± 0.026	19.2 ± 3.9	0.752 ± 0.014	-11.00 ± 0.10	0.460 ± 0.012	-7.85 ± 0.60
γ	$-dF/dt$	0.363 ± 0.028	-13.40 ± 0.60	0.820 ± 0.043	-11.05 ± 0.20	0.504 ± 0.039	-8.50 ± 0.65
γ	$-dE/dt$	0.215 ± 0.043	-13.9 ± 4.1	0.591 ± 0.085	10.8 ± 3.6	0.444 ± 0.061	11.55 ± 0.60
τ^e	C	-0.838 ± 0.021	0.3 ± 1.7	0.426 ± 0.031	-25.55 ± 0.15	0.616 ± 0.022	-60.0 ± 1.7
τ	F	-0.812 ± 0.027	0.5 ± 2.6	0.453 ± 0.045	-25.6 ± 2.1	0.647 ± 0.018	-58.6 ± 5.4
τ	E	-0.933 ± 0.014	0.0 ± 2.1	0.632 ± 0.037	-11.3 ± 8.7	0.734 ± 0.022	-24 ± 21
τ	dC/dt	0.360 ± 0.033	-13.4 ± 3.5	0.748 ± 0.017	-11.00 ± 0.10	0.457 ± 0.014	-8.45 ± 0.60
τ	dF/dt	0.387 ± 0.033	-13.4 ± 2.6	0.777 ± 0.044	-11.2 ± 2.3	0.525 ± 0.044	-10.8 ± 1.0
τ	dE/dt	0.166 ± 0.035	9 ± 19	0.572 ± 0.089	10.8 ± 6.8	0.424 ± 0.060	11.4 ± 2.8

Note. — For Cyg X-1, γ , τ , E , and F are derived based on the relation between γ and the ASM channel ratio (see Equation 1). “ γ ” for Cyg X-3 is replaced by the raw ASM channel ratio, and τ , E , and F cannot be derived, since the spectral shape is complex.

^aPower-law index.

^bRaw count rate (PCA 2.5-25 keV or ASM channels 2+3).

^cFlux, photons $\text{cm}^{-2}\text{s}^{-1}$, 2-100 keV.

^dEnergy flux, ergs $\text{cm}^{-2}\text{s}^{-1}$, 2-100 keV.

^eOptical depth derived from γ (see §3.3).

For Cyg X–1 the PLI and ASM channel ratio were shown to be linearly correlated (Figure 3), and therefore they yield the same curve when scaled to zero mean and unit rms.

Cyg X–1 and Cyg X–3 (Figures 6 and 7) show an extremely good correlation of the PLI with the photon flux or count rate, but no clear correlation with its derivative. 1E 1740.7–2942 (Figure 8, Table 1) shows the opposite behavior: a very good correlation of the PLI with the derivative of the photon flux, and a poor correlation with the flux itself. The PLI leads the flux derivative significantly, i.e. the beginning of an episode of softening is a predictor of a drop in the photon flux. GRS 1758–258 (Figure 9) shows behavior more like that of 1E 1740.7–2942 than that of Cyg X–1, although the correlation with the flux derivative is not as good.

Qualitatively, the results of Figures 6-9 are the same whether the quantity compared to the PLI is the 2-100 keV photon flux as shown or the raw count rate in the instrument (PCA or ASM; see Table 1). When the energy flux from 2-100 keV is used in place of the photon flux, 1E 1740.7–2942 and GRS 1758–258 still show a better correlation with the flux derivative than with the flux, but the correlations are weaker and the sign of the lag is reversed: the energy flux derivative leads the PLI (Figures 10 and 11). The corresponding plot for Cyg X–1 using the energy flux looks similar to the photon flux plot (Figure 6). Because we don’t have a formula like equation 1 to convert the Cyg X–3 ASM channel ratio to a PLI, we don’t calculate the energy flux for Cyg X–3.

We don’t calculate a correlation for GX 339–4 because there is only a single major episode in the plot shown in Figure 4: the rise to the soft state around January 1998 and the fall back to the hard state around December 1998. The first dotted line in Figure 4 shows the time at which the power law becomes soft. The second dotted line shows the time at which it hardens again. Note that at this time the flux has already dropped to a level considerably lower than that at which the power law first softened. Although this is a very small amount of data, qualitatively we might say that GX 339–4 resembles Cyg X–1 during the rise (softening correlated with flux) and 1E 1740.7–2942 and GRS 1758–258 during the decline (a soft spectrum while the flux decreases). It has been noted that some black-hole x-ray nova outbursts have a hard-to-soft transition at high luminosity followed by a soft-to-hard transition at much lower luminosity (Miyamoto et al. 1995). In addition to citing the well-studied x-ray nova GS 1124-683 (Nova Muscae 1991), Miyamoto et al. found evidence for a non-simultaneous change of flux and PLI in GX 339–4 using data taken by several instruments in 1988 and 1991. The total luminosity in the power law spectral component peaked as the PLI was making a transition from -2 to -3.

2.3. The most sudden changes

Although most of the large variations in count rate and PLI in 1E 1740.7–2942 and GRS 1758–258 have been well sampled by our observing program (see Figure 1), each source has on at least one occasion changed too rapidly for us to follow the change in detail. Each of these events is worth special consideration, since the strongest tests of theoretical models for these sources may come from the most extreme variations.

Near the end of 2001 February, the power law flux from GRS 1758–258 dropped by an order of magnitude between one pointing and the next, leaving behind a spectrum dominated by a weak blackbody component. Based on a model of two accretion flows (a sub-Keplerian halo and a thin disk), we predicted (Smith et al. 2001c) that mass input from the companion had ceased, and that the blackbody should decay smoothly over the following weeks. It did so, with a time constant of roughly 28 dy (Smith et al. 2001a). Both the sharp drop (due to the abrupt loss of the power-law component) and the subsequent decay of the soft flux are visible in the count rate plot of Figure 1. This decaying state was similar to the usual black hole “soft” or “high” state, both because it was dominated by thermal emission and because there was no detectable fast x-ray variability. A low-luminosity soft state for this source was previously inferred by Grebenev et al. (1997) from data taken between 1991 Fall and 1992 Spring: during this period, *GRANAT* found only upper limits above 3 keV, while *ROSAT* made a good spectral measurement from 1-2.4 keV. The combined data sets imply that the spectrum had to be both faint and soft. These results differ from the canonical “high/soft” state in that the soft spectrum appears at much lower luminosity than the hard state. The hard to soft transition is usually said to result from an increase in accretion rate and usually involves an increase in luminosity.

A single pointing on 2001 May 14 found that 1E 1740.7–2942 had suddenly jumped from one of softest PLIs ever seen from this source (2.23 ± 0.02) to one of the hardest (1.49 ± 0.02) (Smith et al. 2001b). As can be seen in Figure 12, the 2-100 keV (extrapolated) photon flux remained virtually unchanged while the spectrum hardened, so that the 2-100 keV energy flux briefly doubled, returning at the next pointing to its previous value. The raw PCA count rate (2.5-25 keV) increased slightly (this can be seen in Figure 1). If this one point was taken out of the data, the behavior in this period would be very similar to what we observe at other times: a softening preceding a drop in the photon flux by about 10 dy (see above). We can be fairly certain that the May 14 result is not due to a second, very hard source turning on in the PCA field of view, because the hardening involved not just an increase in high-energy counts, but also a decrease in low-energy counts. Although this may be a rare sort of event, it might also be common but short-lived, and detected only once for that reason.

3. Discussion

3.1. Basic conclusions

Cyg X–1 has long been the prototype which theories of black-hole accretion have tried to model. The results above make it clear that there can be a richer variety of behavior even in other persistent black-hole binaries than is observed in Cyg X–1. Specifically, any model in which a single variable (e.g. a single accretion rate) controls both the luminosity and the spectrum is clearly inadequate to explain the behavior of 1E 1740.7–2942 and GRS 1758–258, even if it is extremely successful with Cyg X–1.

The clearest contrast in behavior is between Cyg X–1 and 1E 1740.7–2942: the PLI correlates with the photon flux in the former and its derivative in the latter. Cyg X–3 is very much like Cyg X–1 in this regard, and GRS 1758–258 is more like 1E 1740.7–2942. More data are clearly needed to place GX 339–4 firmly in either category. In §1, we reviewed the status of knowledge about the companion of each source. For GRS 1758–258, Cyg X–1, and Cyg X–3, we can say that the sources with probable high-mass companions (wind accretors) have the PLI tracking with the flux, and the source with a probable low-mass companion has the PLI tracking the flux derivative. The situation is less clear for GX 339–4 and 1E 1740.7–2942, in the former case because there are not enough data on the x-ray behavior, and in the latter case because there is neither a convincing measurement or upper limit for the companion.

If the correlation between companion type and x-ray behavior holds, the size of the accretion disk may be what distinguishes the two sorts of x-ray behavior. Wind accretors are expected to have a very small specific angular momentum in the accreting material, and therefore should form a very small disk. The complicated behavior in 1E 1740.7–2942 and GRS 1758–258 might then be related to viscous propagation delays that are much smaller in Cyg X–1. For a constant coefficient of kinematic viscosity, ν , the viscous timescale in a standard thin disk $t_{\text{visc}} \sim R^2/\nu$ (Frank et al. 1992), so the accretion disk of Cyg X–1 would only have to be an order of magnitude smaller than that of the LMXRBs to have a timescale < 1 dy; i.e. it could still be over a thousand gravitational radii (R_g) in size. One recent model of wind-fed accretion (Beloborodov & Illarionov 2001) produces a standard hard-state spectrum with a very quickly accreting, “inviscid” disk that is extremely small: only $14R_g$. Compact objects which accrete via Roche-lobe overflow, however, have disks of a size on the order of the binary separation. These large disks have a viscous timescale (spiraling in of matter) which can be on the order of days to months (Frank et al. 1992), and could therefore be related to the time lags between correlated quantities in Figures 8 and 9. The ~ 28 -dy decay of GRS 1758–258 in the soft state (Smith et al. 2001a) may be a direct measurement

of the viscous timescale in that source.

Another significant difference between Cyg X–1 on the one hand and 1E 1740.7–2942 and GRS 1758–258 on the other is that the latter sources have bright radio lobes (Mirabel et al. 1992; Rodríguez, Mirabel, & Martí 1992). This could be a consequence of disk size being related to jet collimation, of disruption of incipient jets by the companion wind in Cyg X–1, or of some other phenomenon. If a substantial fraction of the hard x-ray emission in 1E 1740.7–2942 and GRS 1758–258 occurred in the jets instead of near the disk, one might suggest that the time delays are due to the time required for information about changes in the accretion rate to propagate along the jet to the emitting region (e.g. a shock). The spectrum observed in GRS 1758–258 as its emission shut off early in 2001 (Smith et al. 2001a) eliminates this possibility, however. That spectrum was dominated by a soft thermal component, brighter at first than any that was ever seen in the hard state. Since disk and jet spectral components would simply add, the thermal flux cannot be the jet emission since it is not usually seen in the hard state.

The hard-to-soft transition in Cyg X–1 has sometimes been explained in the context of a central hot, advection-dominated flow with an outer thin disk, the transition radius determined by the accretion rate (e.g., Esin et al. 1998; Janiuk, Życki & Czerny 2000). As the accretion rate increases, the central hot flow becomes unstable to collapse because it can cool itself more efficiently by bremsstrahlung. Here we will refer to this as a “static” soft state, since it can be reached by a gradual, quasi-static change in the accretion rate. In 1E 1740.7–2942 and GRS 1758–258, the softest spectra observed are related to dropping photon fluxes (see Figures 8 & 9). Because the spectral state is related to the rate of change of luminosity, we refer to this as a “dynamical” soft state. Clearly it cannot be related to high accretion rates; GRS 1758–258 showed a soft spectrum down to a few percent of its usual hard luminosity when it shut off (Smith et al. 2001a).

3.2. Relation to previous results

In Paper I, we had only the episodes of brightening and softening occurring in 1E 1740.7–2942 and GRS 1758–258 in 1998 to look at. From these data alone, there was no way to tell whether the PLI was following the same profile as the photon flux but with a delay, or whether it instead followed the flux’s derivative (these options would of course be completely indistinguishable for sinusoidal variations). It is the newer data, including sharp drops in the count rate resulting in more significant softenings, which have decided the question.

We suggested two qualitative models in the Paper I for explaining the lack of simultane-

ity in the variations in flux and PLI. Both pictures involved the simultaneous presence of two accretion flows: a thin Keplerian disk and a hot, sub-Keplerian halo (e.g. an advection-dominated flow (Esin et al. 1998) or a shocked flow (Chakrabarti and Titarchuk 1995)).

Our first picture followed a prediction of Chakrabarti and Titarchuk (1995): the sub-Keplerian flow might exist at all radii, not just within a transition radius, and if the mass accretion rate was boosted to both components at once, the halo would brighten at all radii almost instantaneously (near the free-fall timescale), while the inner regions of the thin disk would only brighten after the extra mass had wound its way in on the viscous timescale. We suggested that when this finally happened, the extra soft photons would cool the halo and the spectrum would soften.

Our second picture followed a suggestion by Mineshige (1996) related to the soft-to-hard state transition in the decaying phase of soft x-ray transients. He suggested that, for accretion rates where both thin-disk and advection-dominated flows are stable, the thin disk may tend to persist once it is established, i.e. the evaporation back to the advection-dominated flow is slow and inefficient. Thus, even if the brightening is quasi-static (i.e. the accretion rate changes slowly compared to the viscous timescale), there can still be a soft stage at the end of the outburst when the accretion rate is low again but the thin disk persists. Most disk analyses concentrate on finding stable solutions; the issue of transformations between stable states is difficult and much less well-explored.

Cyg X–1 provides a perfect test case to distinguish between these two pictures. Since it is expected to have a very short viscous timescale (see above), under the first picture (viscous delay), we would expect a much shorter delay. The second picture (the persistent disk) depends only on a hypothetical property of the inner disk, which should be roughly independent of the outer parts of the accretion flow. Thus, the simultaneity of brightening and softening in Figure 2 causes us to prefer the viscous delay picture (Chakrabarti and Titarchuk 1995) over the slow-evaporation picture for the delay in GRS 1758–258 and 1E 1740.7–2942.

Since we now have considerably more data, showing greater excursions in PLI, a deeper examination of the two-flow picture (Chakrabarti and Titarchuk 1995) is warranted.

3.3. Correlating photon flux and derived halo depth

The hard component in black-hole-candidate spectra has long been attributed to inverse Compton scattering of soft disk photons by energetic electrons, usually but not always thermal. These hot electrons have been hypothesized to reside in several places, often a hot,

central region of the disk or a halo or corona above the disk. The PLI of the Comptonized component is a function of the temperature and optical depth of the Comptonizing plasma. Pietrini & Krolik (1995) have modeled coronae above the disk and found that, for accretion rates much less than Eddington, the halo temperature is nearly constant at a value of about $kT = 100$ keV even as the accretion rate varies by up to four orders of magnitude. A similar result was found by Chakrabarti and Titarchuk (1995), but the hot region was a shocked plasma, originating from a sub-Keplerian flow, and occupying the radially innermost part of the accretion flow. The constant temperature holds as long as the dominant cooling mechanism for the halo is the Comptonization of soft photons and the accretion is significantly sub-Eddington. The highest luminosities derived from the 1E 1740.7–2942 and GRS 1758–258 data of Figure 1 are 9.8 and 5.4×10^{-9} erg cm $^{-2}$ s $^{-1}$ (extrapolated to 2–100 keV and with interstellar absorption removed). For a Galactic Center distance of 8.5 kpc, this gives 8.5 and 4.7×10^{37} erg s $^{-1}$, or about 7% and 4% of the Eddington luminosity for a $10 M_{\odot}$ black hole, so these objects could plausibly be in the constant-temperature regime, in which the PLI depends only on the optical depth τ of the scattering region.

In unsaturated Comptonization, the PLI (Shapiro et al. 1976) is

$$\gamma = \left(\frac{9}{4} + \frac{4}{y(1+f)} \right)^{1/2} - \frac{1}{2} \quad (2)$$

where the spectrum in photons cm $^{-2}$ s $^{-1}$ keV $^{-1} \sim E^{-\gamma}$. The Comptonization parameter

$$y = \frac{4kT_e}{m_e c^2} \text{Max}(\tau, \tau^2) \quad (3)$$

and f is a function only of the halo electron temperature T_e :

$$f = 2.5\theta + 1.875\theta^2(1 - \theta), \quad \theta \equiv kT_e/m_e c^2 \quad (4)$$

which we are taking as constant. Then, at $kT_e = 100$ keV,

$$\tau = 3.3 \left[\left(\gamma + \frac{1}{2} \right)^2 - \frac{9}{4} \right]^{-1} \quad \text{or} \quad 3.3^{1/2} \left[\left(\gamma + \frac{1}{2} \right)^2 - \frac{9}{4} \right]^{-1/2}, \quad (5)$$

whichever is less. With this assumption, τ for 1E 1740.7–2942 and GRS 1758–258 remains close to 1, varying only from 0.44 to 1.39. Since τ increases monotonically as γ decreases, its correlations with photon flux, energy flux, and their derivatives are of the opposite sign and similar magnitude (Figures 13–17 and Table 1).

For an accreting halo flow with an unchanging geometry and constant infall speed, τ is proportional to the accretion rate in this flow, \dot{M}_H . Thus, if the geometry, infall speed, and

temperature of the halo are all constant, the PLI (via τ) is a surrogate for \dot{M}_H . If we could additionally postulate that the photon flux F is a surrogate for the flow in the thin disk, \dot{M}_D , and that the hot halo is an independent flow, then Figures 13-15 could be interpreted in simple and compelling ways. For 1E 1740.7–2942 and GRS 1758–258, where we have a good correlation in the second panel, we would have

$$\tau(t + \delta) - \bar{\tau} \sim \frac{d}{dt}F(t) \quad \rightarrow \quad \dot{M}_H(t + \delta) - \overline{\dot{M}_H} \sim \frac{d}{dt}\dot{M}_D(t), \quad (6)$$

where $\delta < 0$ is the lag shown in Table 1. The mean value is subtracted from τ because of the offset to zero average imposed on all the curves in these figures. This offset has little effect on dF/dt , since it already averages nearly to zero, there being no major long-term trends in the count rates.

Equation 6 suggests that the flow in the thin disk at any time is an integration of the halo flow in the recent past. This would be expected if there were two independent accretion flows: a thin disk (with its slow time constant) and the halo (nearly in free fall), and if they were supplied with proportional amounts of matter at large radii at any given time. The possibility of complicated variations of PLI and luminosity as a result of independent disk and halo flows was predicted by Chakrabarti and Titarchuk (1995). Integration and delay are both natural consequences of viscous propagation in a thin disk (Frank et al. 1992).

Under these assumptions (constant halo temperature and F proportional to disk accretion rate), the observed behavior of Cyg X–1, with a strong inverse correlation in the top panel of Figure 13, could result from

$$\dot{M}_H(t) + \dot{M}_D(t) \sim \text{constant}. \quad (7)$$

In other words, the state transitions could be due to the mass input switching back and forth between going mostly into the halo flow and mostly into the disk. This is an appealing picture of Cyg X–1 for two reasons. First, the bolometric luminosity is, in fact, very nearly constant during state transitions of Cyg X–1 (Zhang et al. 1997), which is not the case for other black-hole candidates. Second, models which attribute the state changes to a change in a single accretion rate (e.g., Esin et al. 1998; Janiuk, Życki & Czerny 2000) require the average accretion rate to be in the narrow range of values near where the hard-to-soft transition naturally occurs. If the state transitions are instead due to the swapping of the accretion flow between two modes, they could occur over a wide range of total accretion rates.

The principal problem with these simple and compelling pictures is the use of F as a surrogate for the thin disk flow. If the thin disk were a point source of soft photons at the center of a large, optically thick Comptonizing cloud, then every photon observed in the

power law would have its origin in the thin disk, and (nearly) every photon emitted by the thin disk would end up in the power law. Such a halo has been postulated by Hua, Kazanas & Cui (1999) to explain the frequency dependence of lags between soft and hard photons at sub-second timescales in black-hole candidates. If the thin disk were a blackbody or a set of concentric blackbodies at different temperatures, then F (first from the thin disk and, after Comptonization, in the power law) would go as $\dot{M}_D^{4/3}$, not very different from \dot{M}_D . For a halo which is close to the disk and tenuous, however, as is sometimes the case in recent models, $\tau \ll 1$, most disk photons are not Comptonized, and F in the power law can be at least as strong a function of \dot{M}_H as \dot{M}_D . A thin halo near the disk also re-heats the disk with some of the Comptonized flux, further complicating the issue. That influence would be lessened if the halo flow were geometrically large, so that most of the Comptonized flux does not intersect the thin disk, or if it had relativistic bulk motion away from the disk, so that the Comptonized photons moved preferentially outward (Beloborodov 1999).

Finally, viscous action in the disk should not only delay but also smooth out variations in the input to the accretion disk. If the F were a good surrogate for the disk accretion flow, it would therefore have less overall variability than the halo flow (represented for the sake of this discussion by τ). This is not the case, however. For $\tau \lesssim 1$, the first exponent in equation 5 is applicable. In this case, the rms variability in τ and in F are remarkably similar. The rms variabilities in F and τ are 19% and 18% respectively in 1E 1740.7–2942 and 22% and 21% in GRS 1758–258. This can't be seen in Figures 14-15 (top panels) because of the scaling used, which automatically sets the rms to 1, but the result is that for $\tau \lesssim 1$ the upper panels in these figures would look the same even without the re-scaling. For $\tau > 1$, the second exponent in equation 5 applies and the problem is aggravated: the rms variabilities in τ are only 9.4% in 1E 1740.7–2942 and 11% in GRS 1758–258, where we would expect them to be higher than the variabilities in F .

On the other hand, the event of 2001 May 14 in 1E 1740.7–2942 (Figure 12) involves both the PLI and energy flux undergoing a large change while the photon flux remains unchanged. This shows that F can sometimes have the slowest response to sudden changes, an expected characteristic of the inner disk accretion rate.

Our purpose, however, is not to argue that a very large, optically thick halo with a uniform temperature actually exists. Rather, it is to stimulate more realistic theoretical work, and to point out that any model of accretion in black-hole binaries must have at least the potential to explain the behavior epitomized by Figure 8. We have used a model of two independent flows and the postulated equivalence in equation 6 as a starting point. In a realistic two-flow model, the observables F and γ would both be functions of both \dot{M}_D and \dot{M}_H . If the two-flow idea is valid, making these relations more physical would result

in maintaining the time lag between \dot{M}_H and \dot{M}_D while making the rms variability of the former greater than the latter.

The disk and halo flows need not have an independent origin as they do in Chakrabarti and Titarchuk (1995). For example, Watanabe & Fukue (1996) discussed how an initially Keplerian corona, produced by evaporation from the disk, could lose angular momentum and accrete rapidly due to radiation drag from a central luminous source (i.e. a neutron star). Greater luminosity from the outer Keplerian thin disk would stabilize against this effect. For a black-hole system, we take the central radiation source as being the innermost region of the disk itself. If the mass input to the thin disk dropped suddenly, the inner disk radiation would at first dominate over the outer disk radiation since the drop would not yet have propagated inward. Thus the corona would accrete more quickly than normal. If the corona is produced at a constant rate by evaporation, the result would be a thinner corona and a softer power-law. Once the drop in accretion rate had propagated to the innermost regions, the former disk/corona ratio would re-establish itself and the spectrum would harden again at a lower luminosity. This reproduces the qualitative behavior in Figures 8 and 9: a softening precedes a drop in flux. What this picture has in common with Chakrabarti and Titarchuk (1995) is the viscous delay in the thin disk as the cause of the complication in the observed behavior.

4. Summary

We have found that black-hole candidates GRS 1758–258 and 1E 1740.7–2942 display long-term behavior very different from the well-known variation of Cyg X–1. The primary result, that the PLI varies as the negative derivative of the power-law flux instead of directly with it, is at least suggestive of a model with both slow (disk) and fast (halo) accretion flows.

Our observations come at a time when there is mounting evidence that even the outer parts of accretion disks contain a vertically extended flow as well as a standard thin disk. Cottam et al. (2001) observed the low-mass x-ray binary EXO 0748–67 with the Reflection Grating Spectrometer on the *XMM-Newton* observatory. Although this is an eclipsing binary, they found very bright x-ray emission lines which do not vary with the variation of the continuum from the central source. From this lack of variability and the details of the absorption and emission in the spectrum, they concluded that there must be a significant flow at large radii with a height much greater than that predicted by hydrostatic equilibrium of a thin disk. Smale et al. (2000) observed another dipping binary, X1624–490, with *RXTE*. They found that the Comptonization region which produces the hard x-ray continuum is never completely occulted during dips, while the blackbody from the central source is. From

the broad profile of the dips, they deduced that the hard-x-ray-emitting region was 5×10^{10} cm in radius or larger, within a factor of two of the full presumed size of the thin accretion disk based on the 21-hour orbit of the system.

Kaaret et al. (1998) described certain correlations in the atoll sources (neutron-star binaries) 4U 0614+091 and 4U 1608–52 that might also be due to independent disk and halo flows. In those sources, the frequency of the kilohertz quasi-periodic oscillations (QPOs) correlates well with the power-law index (Kaaret et al. 1998) and, for 4U 0614+091, with the disk blackbody flux (Ford et al. 1997). Neither these sources, nor the kilohertz QPO sources in general, show a long-term correlation between QPO frequency and luminosity. Kaaret et al. (1998) suggested that the thin-disk accretion rate may control the blackbody luminosity, the QPO frequency, and (via Compton cooling of the halo) the power-law index, while the overall luminosity (dominated by the power-law) is controlled by the halo accretion rate.

Our secondary conclusion is that there can be two causes of spectral softening in black-hole binaries: the well-modeled static soft state, in which the accretion rate becomes high enough to force the innermost part of the halo into the thin disk configuration, and a newly-discovered dynamical soft state, occurring whenever the photon flux is dropping. In the context of a picture of two independent accretion flows, the dynamical soft state would occur when the inner thin disk has yet to respond to a drop in accretion which has already depleted the halo.

Because persistent black hole candidates are rare, there are only a few more immediately available tests of the ideas developed here. LMC X–3 is one source we have not yet examined. It is too faint for the *RXTE* ASM data to be useful spectrally, and the PCA monitoring observations so far, although they have revealed that the source does undergo soft/hard transitions (Wilms et al. 2001), have been too few to provide evidence for or against viscous delay. With a main sequence companion of only modestly high mass (B3 V), it is probably a disk accretor, and may therefore be a good candidate for delays. GX 339–4, which we expect to show delays, may provide more conclusive data than the hint visible in Figure 4. A new PCA monitoring campaign for this source began in 2001 March. Finally, the *XMM-Newton* x-ray telescope has sufficient sensitivity to measure spectra of sources as faint as 1E 1740.7–2942 and GRS 1758–258 in M31 with a reasonable exposure time (< 1 dy). A monitoring campaign of the M31 bulge region could reveal a number of new sources with behavior similar to 1E 1740.7–2942 and GRS 1758–258. If this behavior is indeed due to viscous delay in the disk, this campaign would produce a census of high-mass versus low-mass binaries using viscous delay as a distinguishing diagnostic.

In future work we will consider the connection between the behavior exhibited by

1E 1740.7–2942 and GRS 1758–258 and that observed in the x-ray novae or soft x-ray transients. The transient systems, exemplified by Nova Muscae 1991 (GS 1124–683), tend to brighten in their hard state, change to the soft state near their peak, and decay in the soft state, returning to the hard state only at much lower luminosities (Miyamoto et al. 1995). GX 339–4, much more variable than 1E 1740.7–2942 and GRS 1758–258 but more persistent than the transients, may serve to clarify the connection.

The authors thank two anonymous referees for many useful suggestions and corrections. This work was funded in part by NASA grant NAG5-7265.

REFERENCES

- Beloborodov, A. M. 1999, *ApJ*, 510, L123
- Beloborodov, A. M., & Illarionov, A. F. 2001, *MNRAS*, 323, 167
- Callanan, P. J., Charles, P. A., Honey, W. B., & Thorstensen, J. R. 1992, *MNRAS*, 259, 395
- Chakrabarti, S. K. & Titarchuk, L. G. 1995, *ApJ*, 455, 623
- Churazov, E., Gilfanov, M., & Sunyaev, R. 1996, *ApJ*, 464, L71
- Cottam, J., Kahn, S. M., Brinkman, A. C., den Herder, J. W., & Erd, C. 2001, *A&A*, 365, L277
- Cowley, A. P., Crampton, D., & Hutchings, J. B. 1987, *AJ*, 93, 195
- Esin, A., Narayan, R., Cui, W., Grove, J. E., & Zhang, S. N. 1998, *ApJ*, 505, 854
- Ford, E. C. et al. 1997, *ApJ*, 486, L47
- Frank, J., King, A., & Raine, D. 1992, *Accretion Power in Astrophysics*, 2nd ed. (Cambridge: Cambridge Univ. Press), p. 99
- Gierliński, M., Zdziarski, A. A., Poutanen, J., Coppi, P. S., Ebisawa, K., & Johnson, W. N. 1999, *MNRAS*, 309, 496
- Grebenev, S. A., Pavlinsky, M. N., & Sunyaev, R. A. 1997, in *The Transparent Universe*, Proc. of the 2nd INTEGRAL Workshop, ed. C. Winkler, T. Courvoisier, & P. Durouchoux, (ESA SP-382), p. 183
- Hua, X.-M., Kazanas, D., & Cui, W. 1999, *ApJ*, 512, 793

- Ilovaisky, S. A., Chevalier, C., Motch, C., & Chiappetti, L. 1986, *A&A*, 164, 67
- Jahoda, K. et al. 1996, *SPIE*, 2808, 59
- Janiuk, A., Życki, P. T., & Czerny, B. 2000, *MNRAS*, 314, 364
- Kaaret, P., Yu, W., Ford, E. C., & Zhang, S. N. 1998, *ApJ*, 497, L93
- van Kerkwijk, M. H., Gaballe, T. R., King, D. L., van der Klis, M., & van Paradijs, J. 1996, *A&A*, 314, 521
- Main, D. S., Smith, D. M., Heindl, W. A., Swank, J., Leventhal, M., Mirabel, I. F., & Rodríguez, L. F. 1999, *ApJ*, 525, 901
- Martí, J., Mereghetti, S., Chaty, S., Mirabel, I. F., Goldoni, P., & Rodríguez, L. F. 1998, *A&A*, 338, L95
- Martí, J., Mirabel, I. F., Chaty, S., & Rodríguez, L. F. 2000, *A&A*, 363, 184
- Méndez, M., & van der Klis, M. 1997, *ApJ*, 479, 926
- Mineshige, S. 1996, *PASJ*, 48, 93
- Mirabel, I. F., Morris, M., Wink, J., Paul, J., & Cordier, B. 1991, *A&A*, 251, L43
- Mirabel, I. F., Rodríguez, L. F., Cordier, B., Paul, J., & Lebrun F. 1992, *Nature*, 358, 215
- Mitra, A., 1996, *MNRAS*, 280, 953
- Mitra, A., 1998, *ApJ*, 499, 385
- Miyamoto, S., Kitamoto, S., Hayashida, K., & Egoshi, W. 1995, *ApJ*442, L13
- Nakamura, H., Matsuoka, M., Kawai, N., Yoshida, A., Miyoshi, S., Kitamoto, S., & Yamashita, K. 1993, *MNRAS*, 261, 353
- Phillips, J. A., & Lazio, T. J. W. 1995, *ApJ*, 442, L37
- Pietrini, P., & Krolik, J. H. 1995, *ApJ*, 447, 526
- Pottschmidt, K., Wilms, J., Nowak, M. A., Heindl, Smith, D. M., & Staubert, R. 2000, *A&A*, 357, L17
- Predehl, P., Braeuninger, H., Burkert, W., & Schmitt, J. H. M. M. 1991, *A&A*, 246, L40
- Rodríguez, L. F., Mirabel, I. F., & Martí, J. 1992, *ApJ*, 401, L15

- Sakano, M., Imanishi, K., Tsujimoto, M., Koyama, K., & Maeda, Y. 1999, *ApJ*, 520, 316
- Schmutz, W., Geballe, T. R., & Schild, H. 1996, *A&A*, 311, L2
- Shapiro, S., Lightman, A., & Eardley, D. 1976, *ApJ*, 204, 187
- Smale, A., Church, M. J., & Balucińska-Church, M. 2000, preprint (astro-ph/0010397)
- Smith, D. M., Heindl, W. A., Swank, J., Leventhal, M., Mirabel, I. F., & Rodriguez, L. F. 1997, *ApJ*, 489, L51
- Smith, D. M., Heindl, W. A., Markwardt, C. B. & Swank, J. 2001, *ApJ*, 554, L41
- Smith, D. M., Heindl, W. A., Markwardt, C. B. & Swank, J. 2001, *Astron. Telegram* 69
- Smith, D. M., Heindl, W. A., Markwardt, C. B. & Swank, J. 2001, *Astron. Telegram* 66
- Watanabe, Y. & Fukue, J. 1996, in *Physics of Accretion Disks*, S. Kato, S. Inagaki, S. Mineshige, & J. Fukue, eds., (Gordon and Breach:Amsterdam), p. 223
- Wilms, J., Nowak, M. A., Pottschmidt, K., Heindl, W. A., Dove, J. B., & Begelman, M. C. 2001, *MNRAS*, 320, 327
- Yan, M., & Dalgarno, A. 1997, *ApJ*, 481, 296
- Zdziarski, A. A., Poutanen, J., Mikolajewska, J., Gierliński, M., Ebisawa, K., & Johnson, W. N. 1998, *MNRAS*, 301, 435
- Zhang, S. N., Cui, W., Harmon, B. A., Paciesas, W. S., Remillard, R. E., & van Paradijs, J. 1997, *ApJ*, 477, L95

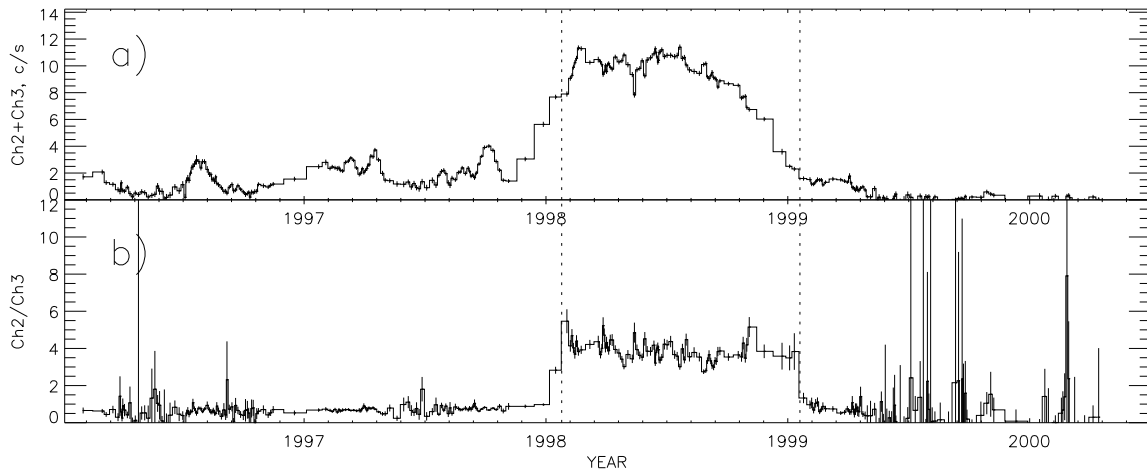


Fig. 4.— Summed count rate in channels 2 and 3 and ratio between channels 2 and 3 (spectral softness) in GX 339–4 from *RXTE* ASM data. Dotted lines show where there is evidence of a slight lag between flux and hardness variation at the state transitions.

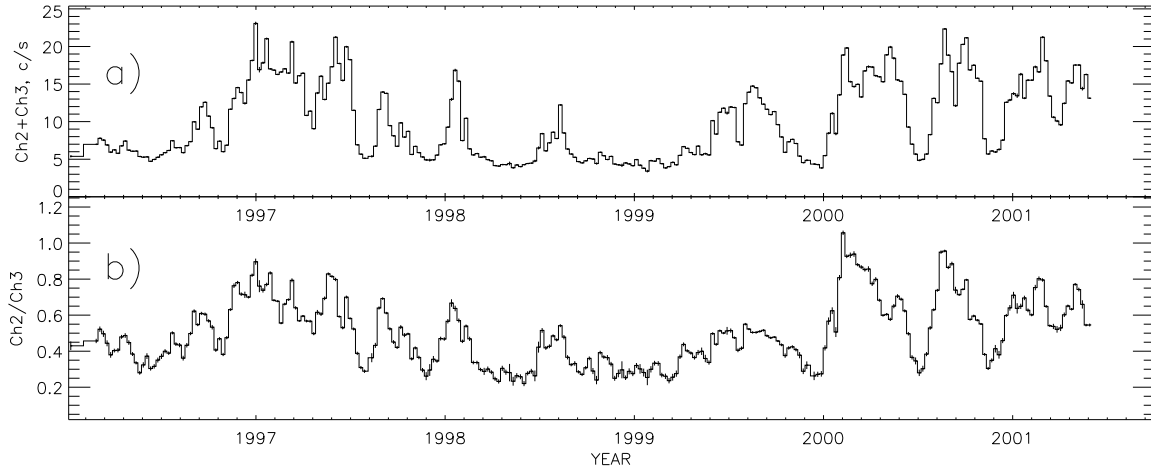


Fig. 5.— Summed count rate in channels 2 and 3 and ratio between channels 2 and 3 (spectral softness) in Cyg X-3 from *RXTE* ASM data.

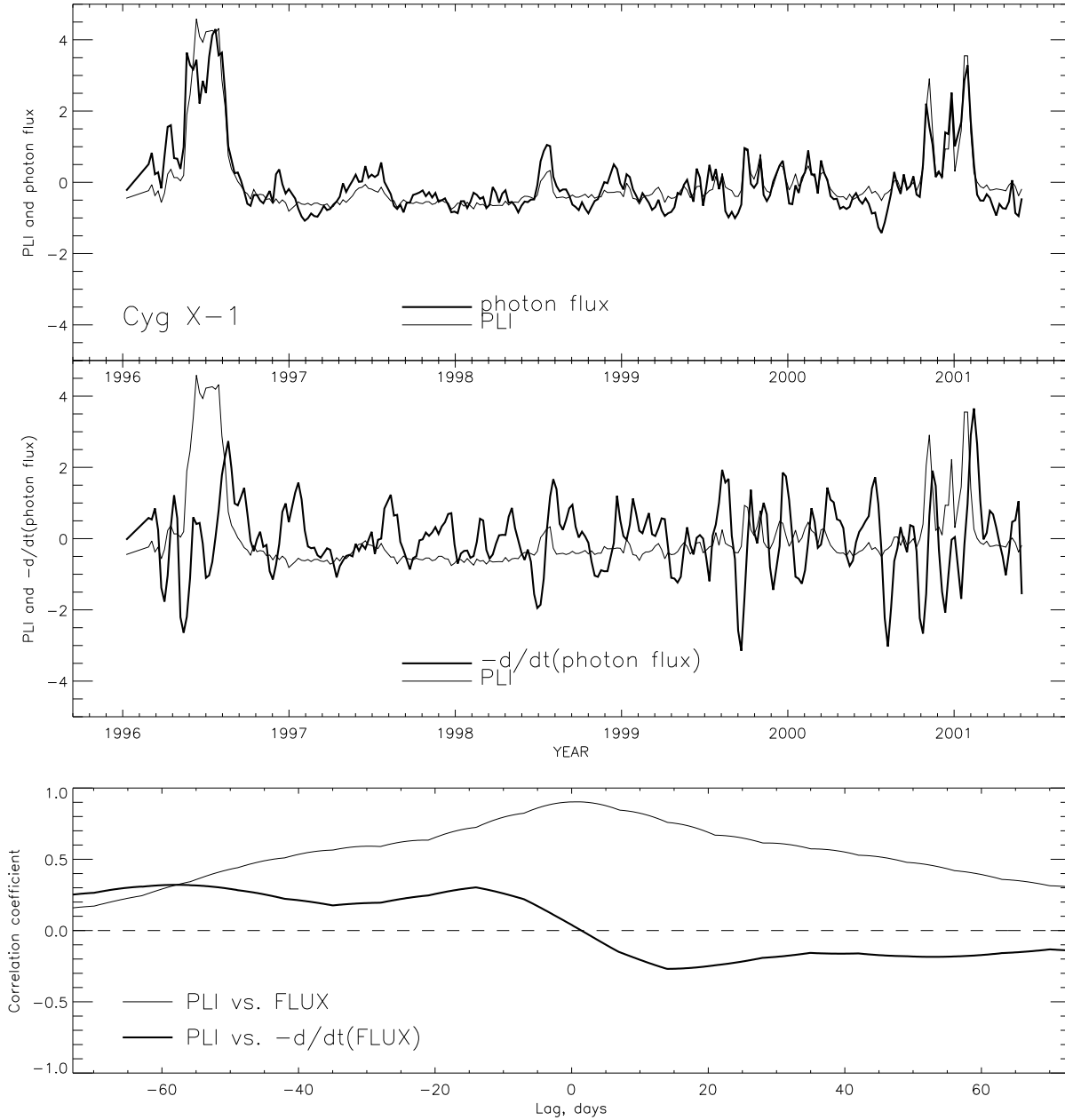


Fig. 6.— Top panel: Scaled curves of PLI and photon flux for Cyg X-1 (see text). Middle panel: Scaled curves of PLI and minus the time derivative of the photon flux. Bottom panel: correlation coefficient vs. lag for each of the two sets of curves.

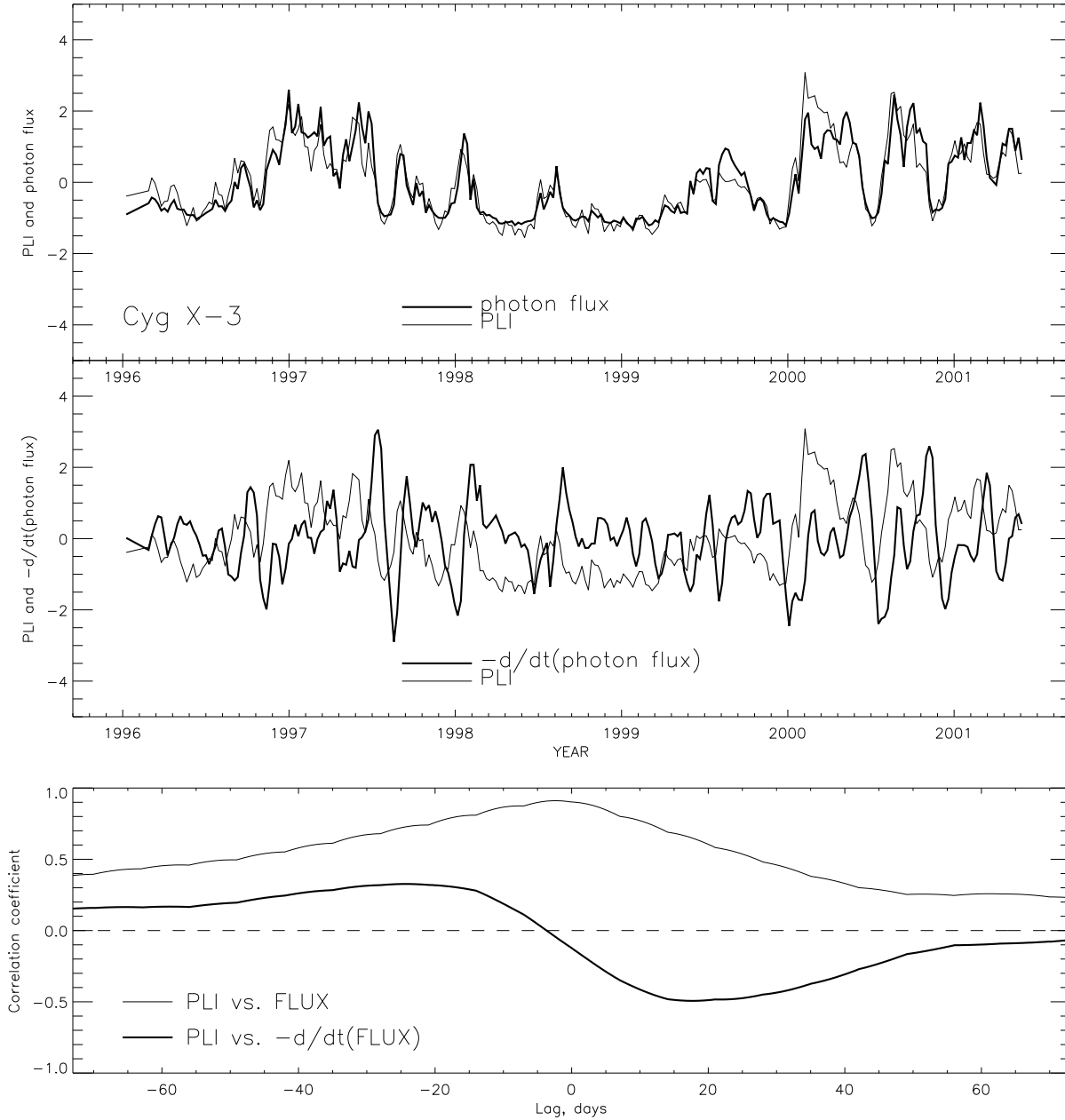


Fig. 7.— Same as Figure 6 but for Cyg X-3, with the count rate ratio of ASM channel 2 to ASM channel 3 in place of the PLI.

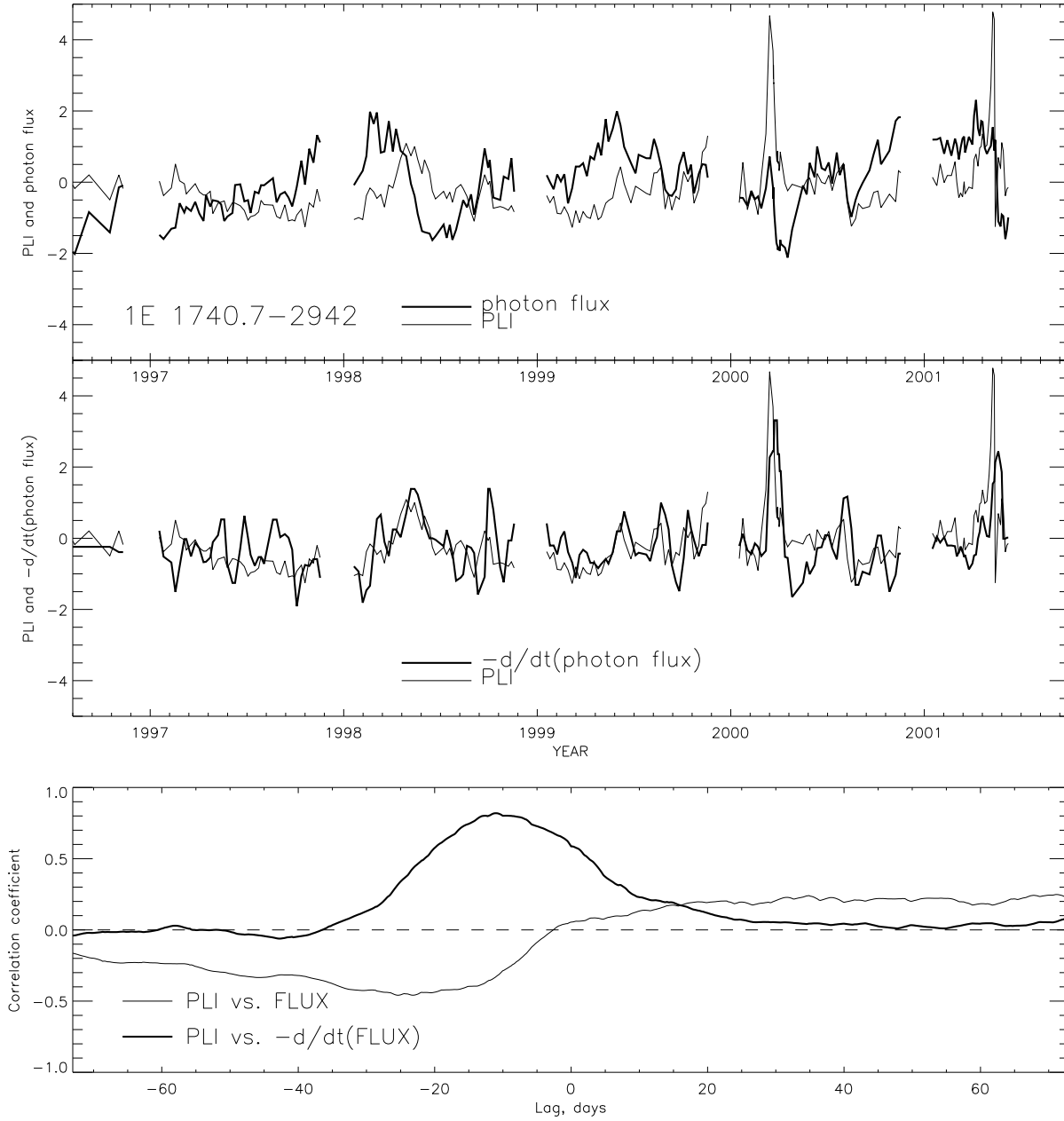


Fig. 8.— Same as Figure 6 but for 1E 1740.7-2942.

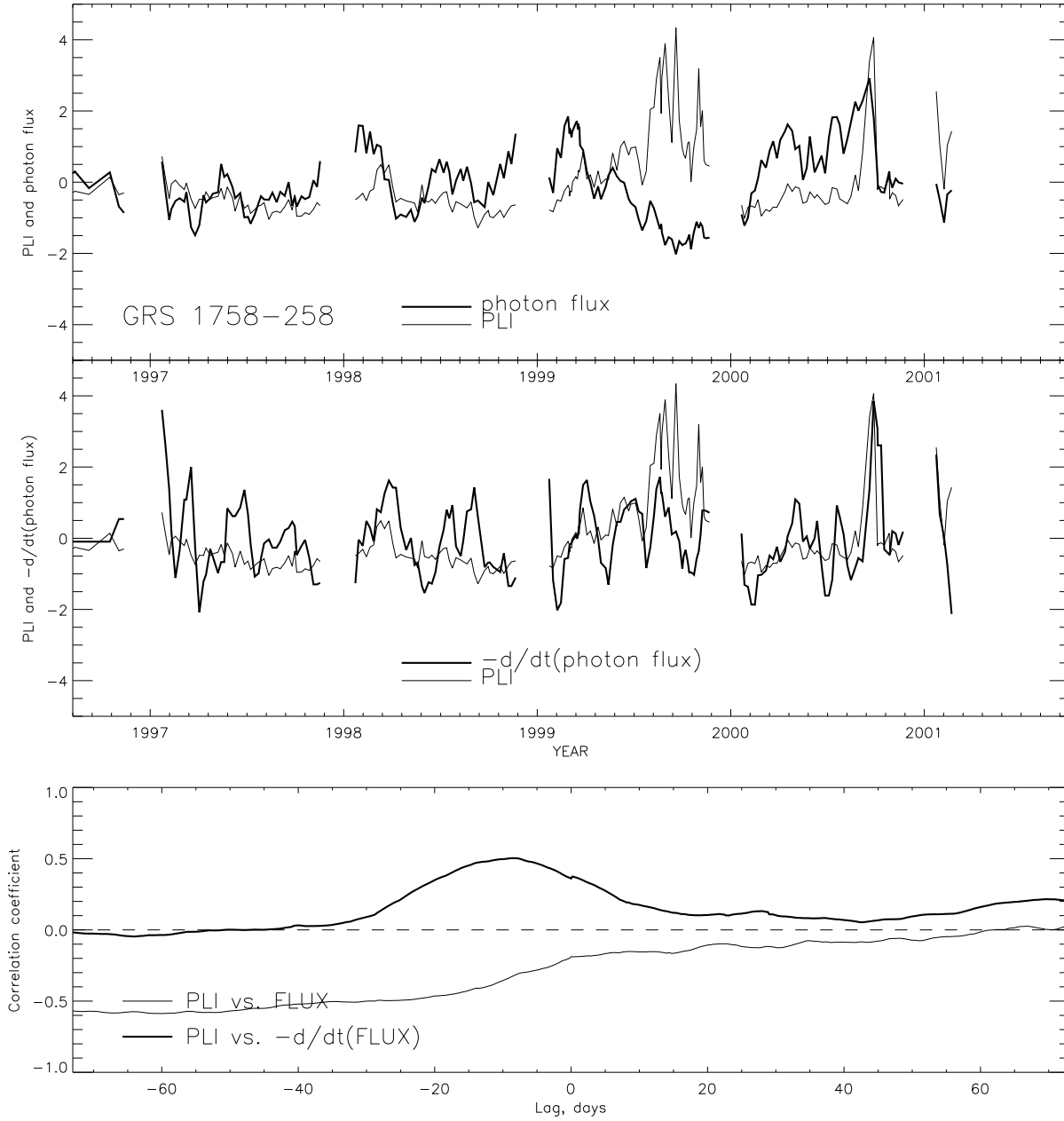


Fig. 9.— Same as Figure 6 but for GRS 1758-258.

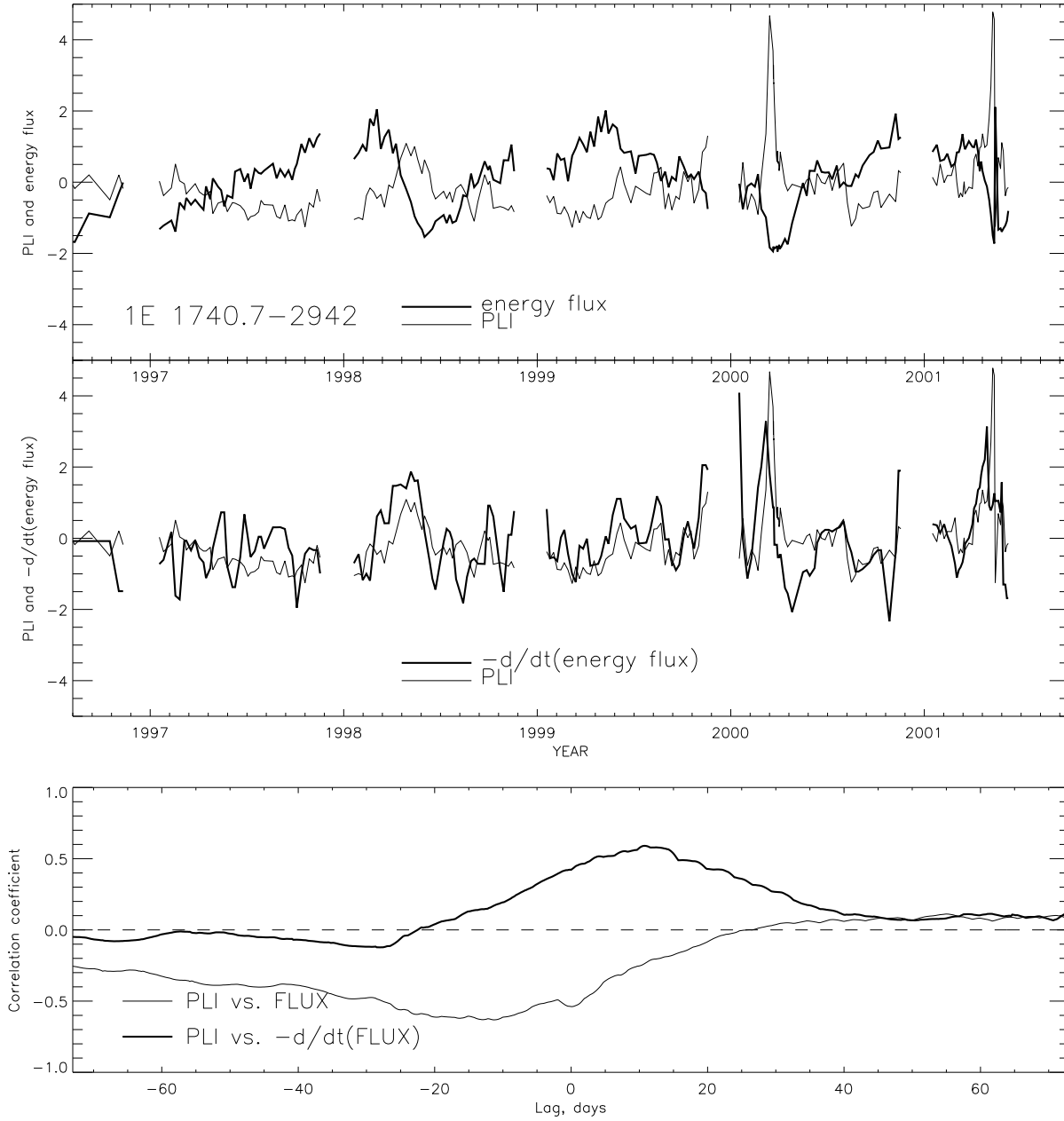


Fig. 10.— Same as Figure 8 but with energy flux (2-100 keV) in place of photon flux.

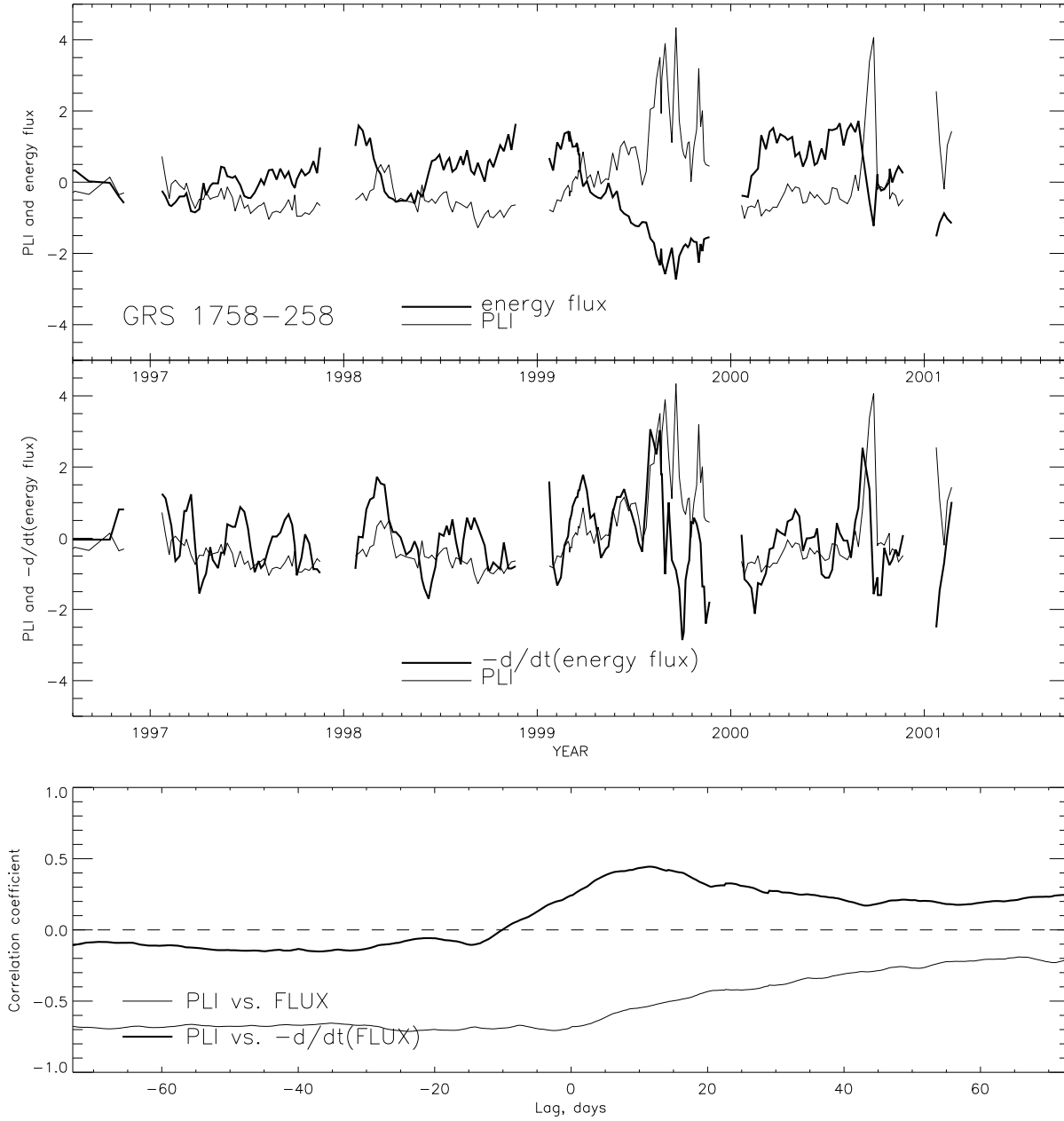


Fig. 11.— Same as Figure 9 but with energy flux (2-100 keV) in place of photon flux.

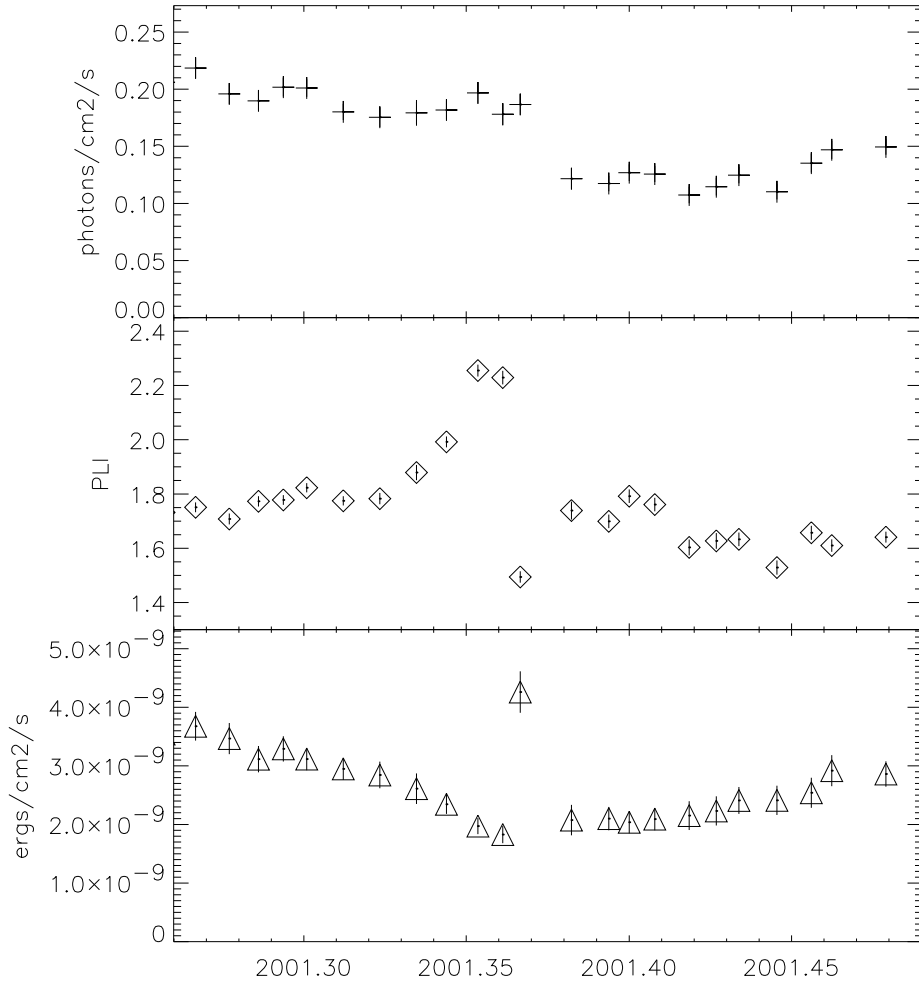


Fig. 12.— Evolution of photon flux (2-100 keV), PLI, and energy flux (2-100 keV) as a function of time around the episode of sudden hardening in 1E 1740.7–2942 on 2001 May 14.

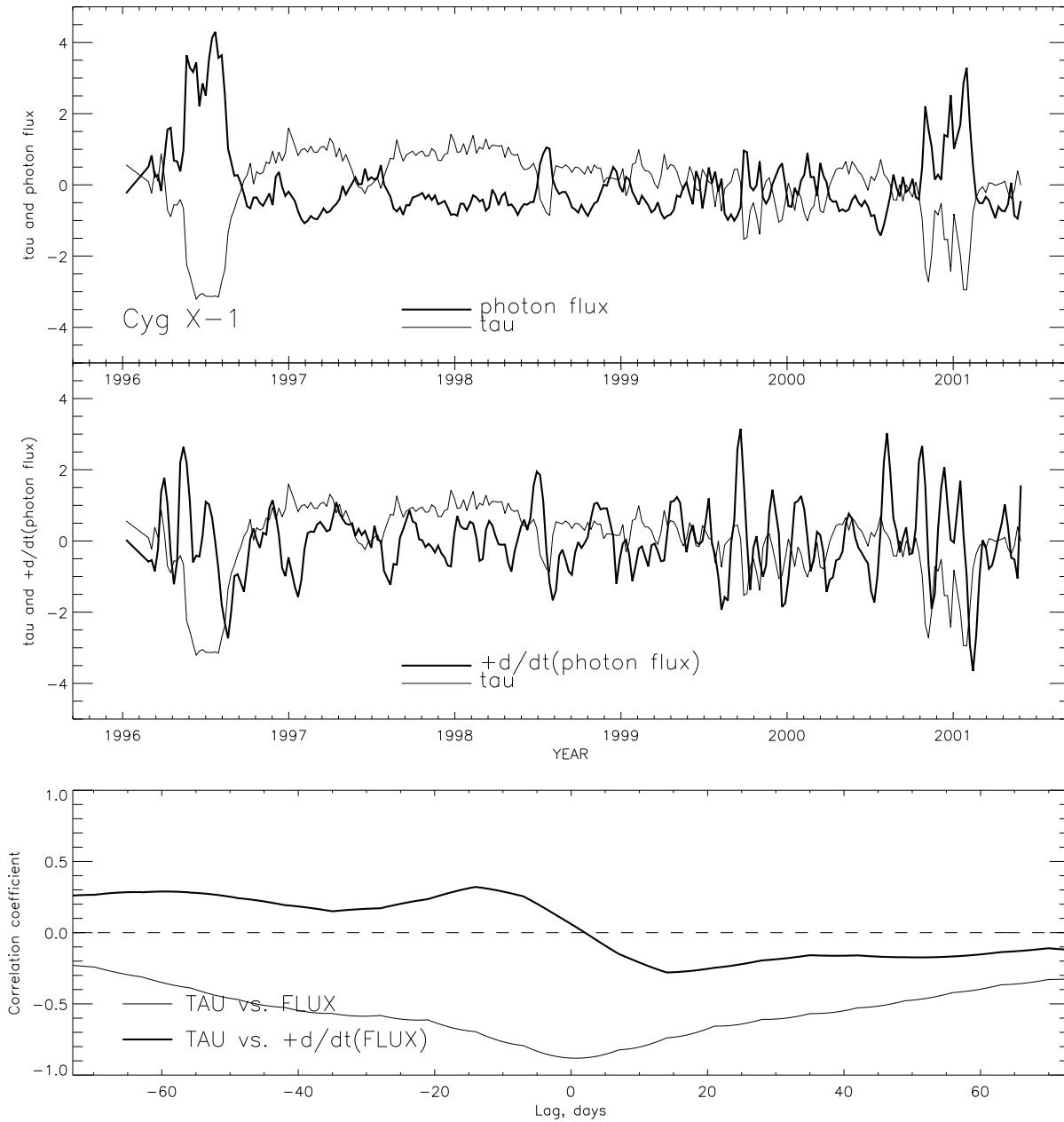


Fig. 13.— Same as Figure 6 but with the PLI replaced by the derived optical depth τ and the flux derivative shown with the opposite sign.

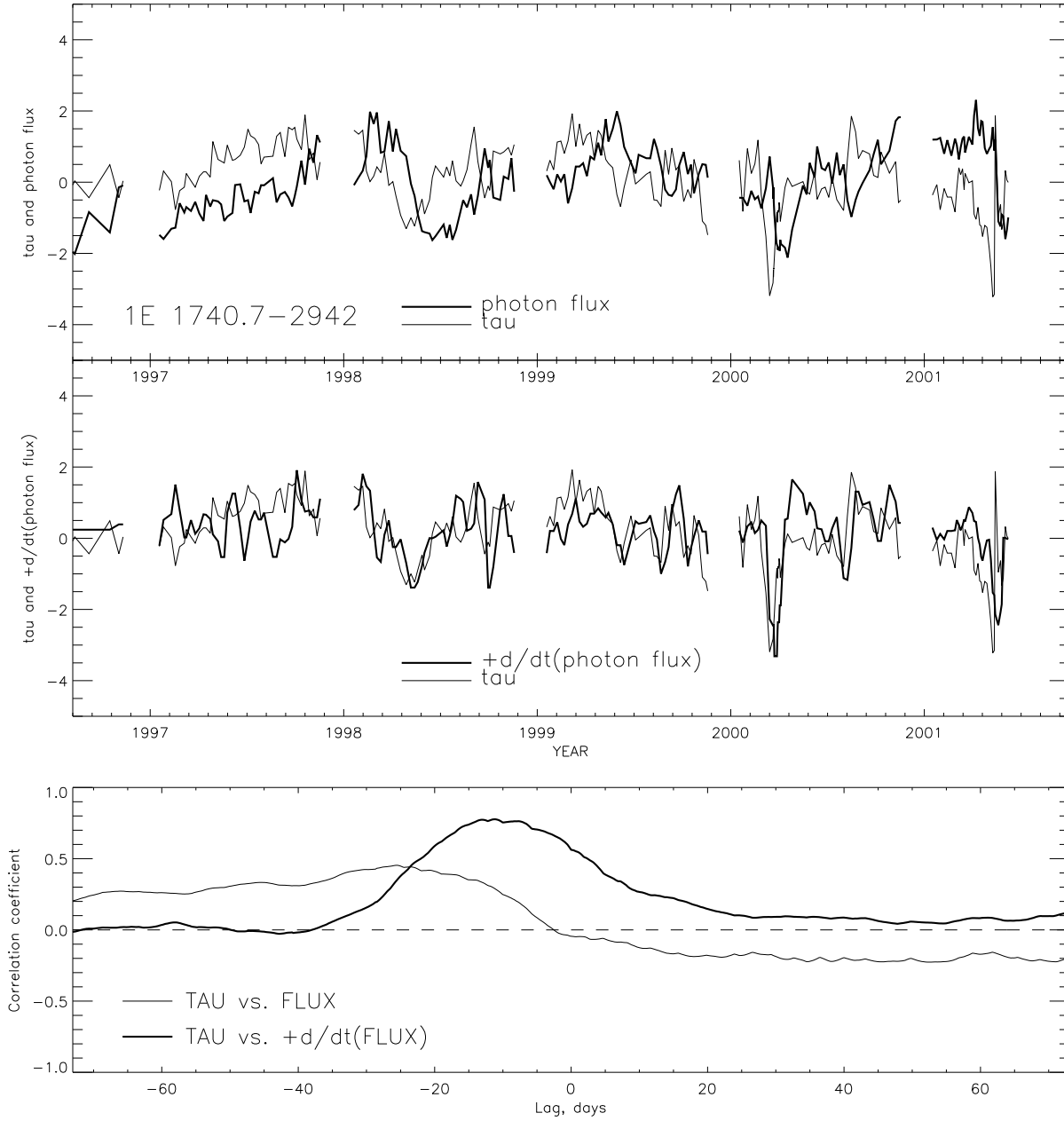


Fig. 14.— Same as Figure 8 but with the PLI replaced by the derived optical depth τ and the flux derivative shown with the opposite sign.

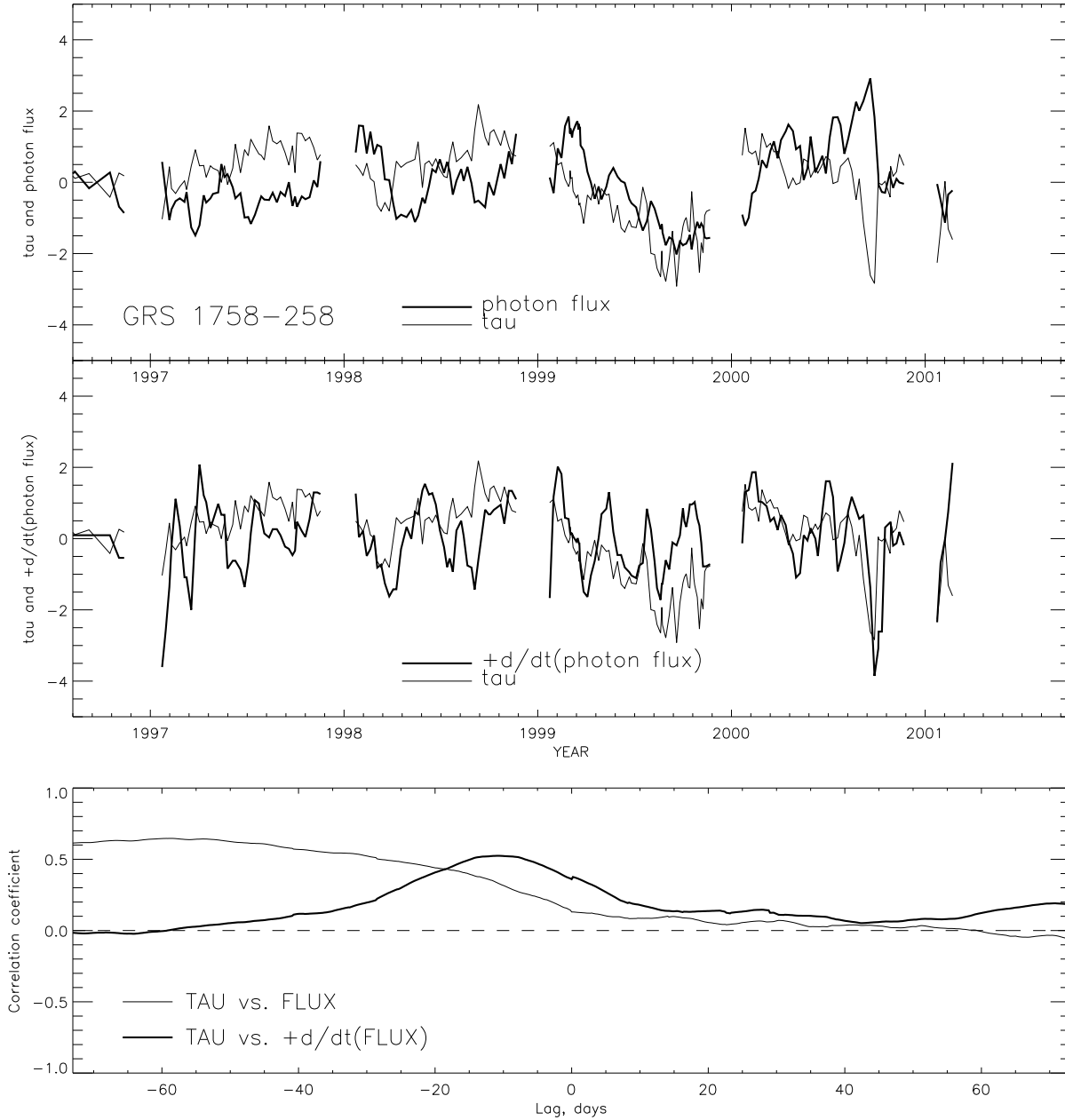


Fig. 15.— Same as Figure 9 but with the PLI replaced by the derived optical depth τ and the flux derivative shown with the opposite sign.

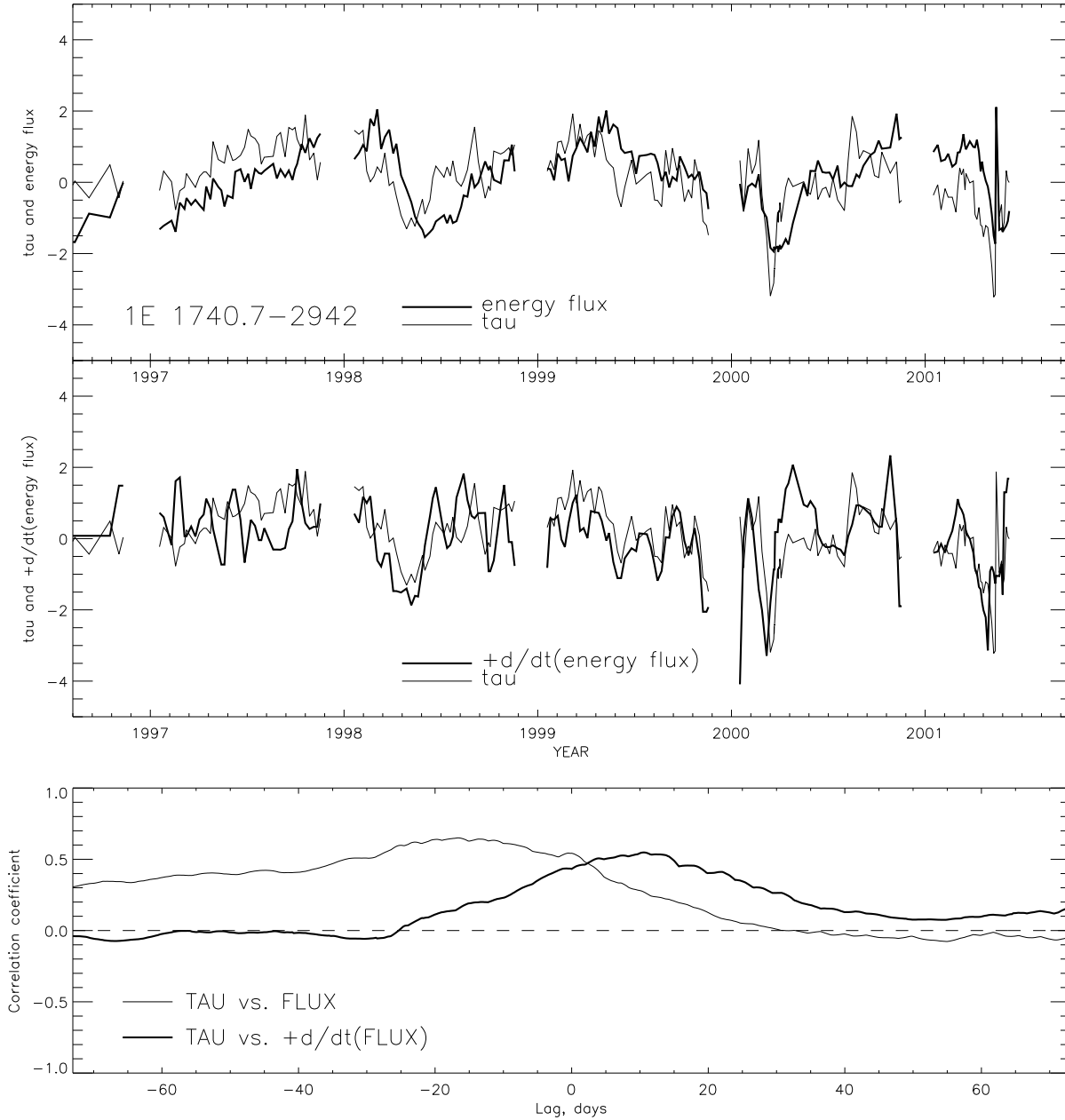


Fig. 16.— Same as Figure 14 but with energy flux (2-100 keV) in place of photon flux.

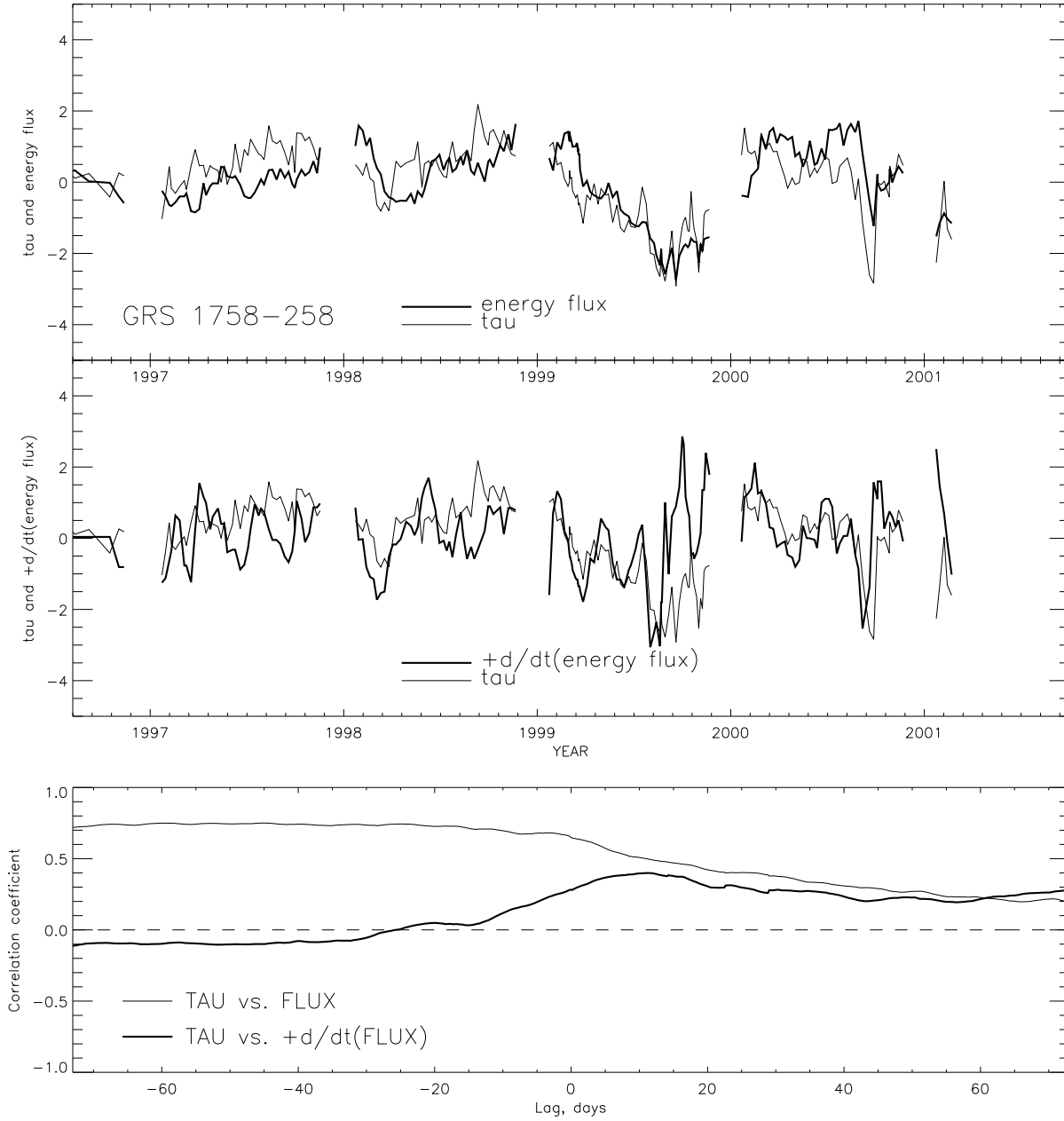


Fig. 17.— Same as Figure 15 but with energy flux (2-100 keV) in place of photon flux.